JMEPEG (2016) 25:3330–3347
DOI: 10.1007/s11665-016-1990-y

1059-9495/$19.00

Critical Issues for Producing UHTC-Brazed Joints: Wetting and Reactivity

A. Passerone, M.L. Muolo, and F. Valenza

(Submitted November 30, 2015; in revised form January 19, 2016; published online March 4, 2016)

A brief survey is presented of the most important interaction phenomena occurring at the solid-liquid interfaces in metal-ceramic systems at high temperatures, with special attention to the most recent developments concerning wetting and joining transition metals diborides. These phenomena are described and discussed from both the experimental and theoretical points of view in relation to joining ceramic and metal-ceramic systems by means of processes in the presence of a liquid phase (brazing, TLPB etc.). It is shown that wetting and the formation of interfacial dissolution regions are the results of the competition between different phenomena: dissolution of the ceramic in the liquid phase, reaction and formation of new phases at the solid-liquid interface, and drop spreading along the substrate surface. We emphasize the role of phase diagrams to support both the design of the experiments and the choice of active alloying elements, and to interpret the evolution of the system in relation to temperature and composition. In this respect, the sessile-drop technique has been shown to be helpful in assessing critical points of newly calculated phase diagrams. These studies are essential for the design of joining processes, for the creation of composite materials, and are of a particular relevance when applied to UHTC materials.

Keywords brazing, ceramics, diborides, joining, phase diagrams, structural, wetting

1. Introduction

Joining ceramic materials, to each other or to high-performance alloys, is of particular interest for many demanding technological applications. Brazing in particular, which involves the presence of a liquid metallic phase in contact with the adjoining phases at high temperatures, requires many critical issues to be studied, such as wetting, dissolution, and reactivity. They must be examined in detail in order to achieve reliable bonding procedures and products.

The attention in this paper will be focused on the issues related to joining transition metals diborides, a class of materials less extensively studied with respect to oxides: they are classified within the class of ultra-high-temperature ceramics (UHTC's), of particular interest for advanced applications (Ref 1).

Transition metals ceramic diborides, such as hafnium, titanium, and zirconium diborides, are members of a family of materials with extremely high melting temperatures, high thermal conductivity, good electrical properties, excellent thermal shock resistance, and high hardness (Ref 2, 3). However, their chemical inertness fails, in the "pure" status in terms of oxidation at high temperature, so that it has been found necessary to add other components, such as SiC, B_4C, $MoSi_2$ to obtain good performances (Ref 4-6).

Use of these materials is currently being considered in the aerospace industry for hypersonic vehicles, atmospheric re-entry, and rocket propulsion (Ref 7-9) where high temperatures, high heat fluxes, and severe surface stresses are involved (Ref 10-13). The unique combination of their properties makes them also suitable for other applications including nuclear plants (Ref 14, 15), solar plants (Ref 16), refractory linings (Ref 17), electrodes (Ref 18-20), microelectronics (Ref 21), and cutting tools (Ref 22).

Ceramic/metal joining is of great technological significance because, by using this process, the individual characteristics of the two types of materials can be used to produce new components with improved performances.

Liquid-phase bonding processes, including brazing (Ref 23-25), and the transient liquid-phase bonding (TLPB) technique (Ref 26-34), are widely used for joining ceramics. In addition, a revival of metal-ceramic bonding via glass- and glass-ceramic phases has been appearing in literature, due to their thermal expansion characteristics, oxidation resistance, and easy processing (Ref 35-40). Therefore, investigations on wetting, spreading, and interfacial behavior in metal/ceramic systems (Ref 41-46, 71), joining processes, and joint performances (Ref 47-54) have become essential.

There follows an overview of recent findings on joining diboride-ceramic materials, preceded by a reminder of the principal interaction phenomena occurring at the solid-liquid interfaces at high temperatures. This is followed by a review of the most recent results concerning their wettability, as the first step toward defining reliable brazing procedures.

2. Wetting

Brazing, a process involving the presence of a liquid phase at high temperature, depends strongly on the complex wetting

This article is an invited submission to JMEP selected from presentations at the Symposium "Wetting and High-Temperature Capillarity," belonging to the Topic "Joining and Interfaces" at the European Congress and Exhibition on Advanced Materials and Processes (EUROMAT 2015), held September 20–24, 2015, in Warsaw, Poland, and has been expanded from the original presentation.

A. Passerone, M.L. Muolo, and **F. Valenza,** IENI-CNR, Via de Marini, 6, 16149 Genoa, Italy. Contact e-mail: a.passerone@ge.ieni.cnr.it.

phenomena occurring at the solid-liquid interface. In order to understand what may happen at this interface, the following processes must be taken into consideration: (a) dissolution of the solid into the liquid, (b) penetration/diffusion of the liquid components into the solid, (c) adsorption of components of the liquid phase at the interfaces, (d) reaction of some component of the liquid with the solid and the formation of new phases, and (e) dynamic restructuring of the solid surface.

All these processes are the result of atom movements, each one of them with its characteristic time (depending on diffusion coefficients and/or reaction rates and, thus, on temperature) which in turn affects the equilibration kinetics, i.e., the overall wetting process.

The adhesion between liquid metals and ceramic materials is due to the type (chemical or metallic bonds, van der Waals) of interactions that can be established between the atoms of the liquid metal phase and those constituting the ceramic body: those at the metal-ceramic interface and the metal-metal ones. An efficient way to study these interactions and to quantify their effects in terms of adhesion energy is offered by modeling (Ref 55-57), through molecular dynamics approaches, or by applying the density functional theory (DFT) (Ref 58-65). In particular, the DFT allows the electronic properties of a system to be obtained starting from its individual constituents (nuclear and electronic charges), in principle "ab initio," without empirical assumptions on the model. Up to now, most efforts have been concentrated on modeling metal/oxides interfaces, but a few calculations exist on metal/carbides (Ref 60, 66, 67), metal/nitrides (Ref 68-70), and metal/borides (Ref 71, 72) systems, arriving at a correct estimation of the metal-ceramic bonding mechanisms. These calculations, applied to the (Au, Ag)/ZrB_2 system, have shown an increase of the overlap between the density of states of Au and Zr at the Fermi energy, indicating the presence of a metallic bonding at the solid-liquid interface (Ref 73). More recently, interfaces of diborides with aluminum (Ref 72) and tungsten (Ref 74) have been studied theoretically with similar methods. These efforts have indeed opened new important insights into the basic solid-liquid interactions at high temperatures.

3. Wetting Typologies

The fundamental equations describing the wetting conditions are the Young relationship:

$$\sigma_{SV} = \sigma_{SL} + \sigma_{LV}\cos\theta, \qquad \text{(Eq 1)}$$

where σ_{SV}, σ_{SL}, and σ_{LV} represent the equilibrium, at the triple line, of the solid-vapor, solid-liquid, and liquid-vapor interfacial tensions through the contact angle θ, and the Work of Adhesion (Young-Dupré equation):

$$W_a = \sigma_{SV} + \sigma_{LV} - \sigma_{SL} = \sigma_{LV}(1 + \cos\theta) \qquad \text{(Eq 2)}$$

the thermodynamic quantity describing the effectiveness of the solid-liquid bond. All relevant relationships describing wetting and contact angle measurements can be found in (Ref 75, 76).

In general, three main wetting categories can be recognized: (a) non-reactive (or adsorptive) wetting, (b) dissolutive wetting, and (c) reactive wetting.

3.1 Non-reactive (or Adsorptive) Wetting

Non-reactive wetting is a modality that can only seldom be invoked to describe completely high-temperature processes, and occurs if certain conditions are met. Indeed, non-reactive wetting can take place, provided the interplay of the three interfacial tensions allows a low-contact angle to be established (as computed by Eq 1), as long as, at the same time: (a) no chemical reactions take place between the liquid and solid phases, (b) the solid and the liquid phases are mutually immiscible, and (c) the liquid phase is in chemical equilibrium with the solid (i.e., it is saturated of the solid elements). These conditions are more easily met if the temperature is not high enough to allow for a sufficiently fast exchange of atoms by diffusion between the solid and the liquid phase.

The spreading process, i.e., the displacement of the triple line according to time, may be fast if compared to dissolution processes, so that the liquid front moves on a flat, unmodified surface (Ref 77). In these cases, the friction at the triple line is the main factor governing the kinetics of the process and, in the case of liquid metals, the overall process can be completed within a few dozen milliseconds.

A study on the kinetics of spreading from the very first instant of solid-liquid contact can offer a means to understand which phenomenon is prevalent in the specific process. However, especially at high temperatures, the experimental part is very difficult, although high-speed recording is now close at hand. What is still lacking is the possibility to access an "in situ" analysis of the interface, which is usually studied after drop solidification; thus when the wetting process is finished, a large number of chemical reactions and/or precipitation phenomena have occurred. Studying the kinetics of spreading is a very complex subject, and a systematic overview of this phenomenon is outside the scope of this paper; however, the interested reader is referred to recent specialized papers (Ref 78-87).

3.2 Dissolutive Wetting

As already mentioned, at a high-temperature, high atom mobility implies that at least some dissolution of the solid phase into the molten matrix can take place until the chemical potential of the diffusing species is the same in the solid and the liquid phases (Ref 77, 85, 88-96). Even if no reactions occur, the composition of the liquid phase changes with time. As a consequence, its surface tension also changes and a dynamic condition is setup, where both contact angle and drop dimensions (base diameter, height, and also volume) are a function of time. The solid-liquid interface no longer lies on a plane, but a groove forms under the drop with a nearly spherical profile (Fig. 1) that can be to some extent perturbed. As an immediate consequence, the Young law (Eq 1) which refers to rigid, homogeneous, non-deformable surfaces, is no longer valid, as the triple line equilibrium must also take into consideration the vertical components of the surface tension vectors. Indeed, the interfacial tension vectors reach an equilibrium configuration at the new triple line expressed by the so-called Neumann rule (Fig. 1):

$$\frac{\sigma_{SL}}{\sin\theta_1} = \frac{\sigma_{SV}}{\sin\theta_2} = \frac{\sigma_{LV}}{\sin\theta_3}. \qquad \text{(Eq 3)}$$

Thus, in this case, what is measured in a sessile-drop test is the "apparent" contact angle, that is the one "above" the plane

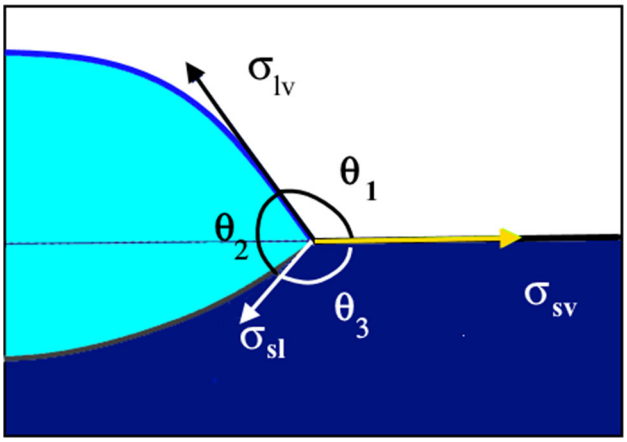

Fig. 1 Equilibrium configuration in the presence of dissolution of the solid

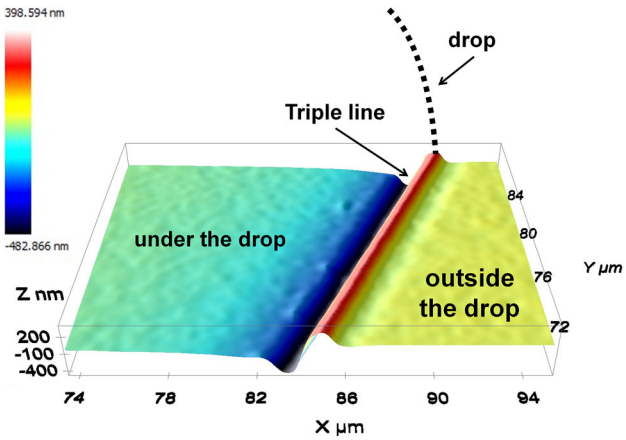

Fig. 2 3D confocal profile of the surface of sapphire after contact with molten Ni at 1500 °C and removal of the drop. The scan reveals the presence of a ridge located at the triple line junction (h 250 nm), and of deep groove (depth ≈ 400 nm) adjacent to it

defined by the solid surface (i.e., π-θ_1 in Fig. 1). This point is extremely important when interpreting sessile-drop results, as any quantitative utilization of contact angle data, especially to derive thermodynamic quantities such as the work of adhesion, should take this effect into serious consideration.

The dissolutive stage of the wetting process is usually very fast. Furthermore, as noted for instance in (Ref 88), dissolution is often increased by soluto-capillary Marangoni movements occurring near the triple line. These processes, discussed in the next paragraph, can lead to the appearance of irregular (“non-Laplacian”) curvatures (Ref 90) and/or to “ridges” a micrometer in size (Fig. 2) at the solid-liquid interface close to the triple line. They have been shown to occur, at the microscopic scale, in many systems at high temperature, even with high melting point ceramic materials and with systems which, at the macroscopic scale, are considered as non-reactive (Ref 78, 82, 97-102). For example, for the Ni-Al_2O_3 system, ridges and grooves, a nanometer in size (Fig. 2) form at the solid-liquid interface close to the triple line.

Considering that the dissolution process should in principle change the liquid-vapor and the solid-liquid surface tensions, a contact angle varying with time should result. As the drop

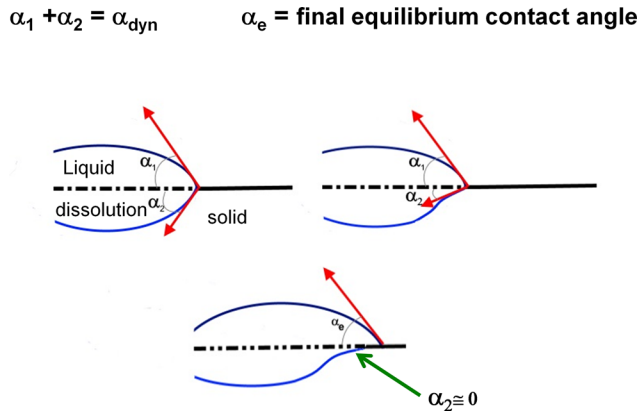

Fig. 3 Evolution of a drop in the presence of dissolution

spreading and the dissolution processes proceed, the amount of solid phase dissolved into the liquid becomes smaller and smaller. In this way, the solid dissolution and thus the depth below the original surface decreases while the base diameter of the drop increases. In addition, if the new angle is lower than the initial one, as soon as it reaches a critical value which allows “depinning” to take place, the (already saturated) liquid drop may spread over the solid surface with the triple line lying outside the dissolution crater, giving rise to a characteristic sigmoidal profile (Fig. 3) (Ref 103).

3.3 Soluto-Capillarity Effects

The well-known dependence of surface tension on temperature T and concentration C makes it possible for L/V interfacial gradients in these physicochemical variables to induce thermo- and soluto-capillary effects, respectively. The role of thermocapillary in spreading drops was analyzed by Erhardt and Davis (Ref 104). They found that, for drops spreading on substrates whose temperature was greater than that of ambient atmosphere, thermocapillary induced a L/V interfacial flow from the triple line to the drop apex. This thermocapillary flow inhibited wetting. Conversely, they found that for drops spreading on substrates whose temperature was less than that of ambient atmosphere, thermocapillary induced an L/V interfacial flow from the drop apex to the triple line; this thermocapillary flow enhanced wetting.

In high-temperature capillarity experiments, the temperature distribution between drop-substrate and ambient depends on the technique used (contact heating, dispensed drop method), on the working atmosphere (vacuum or protective gases), and on the intrinsic properties of drop and substrate (heat capacity, reflectivity etc.) so that no general behavior can be foreseen.

Soluto-capillary effects are much more likely to influence wetting in metal-metal systems when the substrate metal is strongly tensioactive. As an example, (Ref 89) reports wetting in the Cu-Si system. At 1100°C, when the reactive wetting regime is reached, as a first-order approximation one may assume that, due to dissolution, the concentration of Si at the triple line is that of a saturated Cu-Si solution (σ_{lv} = 840 mN/m) and that at the drop apex is close to zero (i.e., pure Cu, σ_{lv} = 1280 mN/m). The resulting soluto-capillary flow on the L/V interface is then from the triple line to the drop apex and wetting is inhibited. The resulting mass transport due to viscous coupling between the L/V interfacial liquid and bulk liquid in the drop can transfer liquid from the triple line region to the drop apex.

It can thus be safely stated that at the beginning of the dissolutive stage, the solutal Marangoni driving force is strong enough to account for the required values of the mass transfer parameter. It should of course be borne in mind that the intensity of convection will decrease during the experiment as a result of the solute enrichment caused by the dissolution itself and by the reduction in the drop thickness due to wetting.

Bulk convection due to density gradients was found (Ref 90) to be negligible with respect to the surface tension-driven Marangoni convection. Furthermore, only solutal Marangoni convection, due to composition gradients along the drop upper surface, was able to provide the large fluid velocities necessary to account for the high value of the mass transport parameter.

3.4 Reactive Wetting

Reactive wetting, proper, means that chemical interactions occur at the solid-liquid interface, with the production of new species which can, in turn, profoundly modify the wetting behavior of the system, through the formation of interfacial new phases that have different wetting characteristics. Literature contains much debate, especially as regards the role that the free energy of reaction can have on the final contact angle. Good reviews/viewpoints on this topic can be found in Ref 101, 103, and 105-107. In the presence of reactions, the final equilibrium configuration should be determined by the formation of continuous layers of specific reaction products, such as the M_6X metal-like compounds in metal-oxide systems (Ref 108, 109), in case of wetting of carbides (Ref 110), or borides, as in the cases dealt with in this paper (see paragraph 5). Which compound can form depends both on the chemistry of the system and on the kinetics of the advancement of the triple line. Indeed, if the presence of minor elements, such as the active elements used in brazing processes (e.g., Ti, Zr, Cr, V, Nb, Al), in the liquid phase can give rise to interfacial reactions whose type and extent depend on the activity of these elements in the experimental conditions, the formation of new compounds through heterogeneous nucleation at the S/L interface can only occur when a certain amount of supersaturation in the liquid phase is reached. In particular, this is more likely to occur when the triple line velocity is very low (Ref 111). Once a continuous layer of the new compound is formed at the S/L interface, the atoms necessary to feed the reaction must be transferred through the layer by solid-state diffusion, with a substantial reduction of the rate of substrate dissolution.

4. Role of the Solid Surface in Modifying the Wetting Behavior

Wetting of solid surfaces is affected, not only by the mechanisms which are behind the wetting typologies already discussed, but also by "physical" and "chemical" factors intrinsic to the solid surface, that are briefly discussed below.

4.1 Roughness

The solid surfaces used in wetting experiments are not ideal. Especially when working at high temperature with polycrystalline materials, surfaces are not perfectly smooth. Ceramic materials are usually produced by sintering. This means that a residual porosity is always present and that, even after a very careful polishing procedure, a residual surface roughness is still present. This residual roughness should be kept within R_a (the arithmetic average of the absolute profile heights) values of the order of a few dozen nanometers. In addition, with rising temperature, micro-faceting and thermal grooving at grain boundaries take place, so that the real roughness conditions governing the wetting process at the test temperature often remain as an unknown parameter.

Roughness affects the establishment of the contact angle by various mechanisms: (a) by increasing the solid-liquid contact area (increase of interfacial energy), (b) by providing "pockets" of entrapped vapors, thus forming a composite interface, (c) by offering specific nucleation points for reaction and growth when reactions can occur, (d) by offering specific "pinning" points to the movement of the triple line.

Wenzel (Ref 112) proposed the following equation for rough surfaces, linking the "macroscopic," measured, contact angle θ_m to the "intrinsic" one θ^*:

$$\cos\theta_m = \boldsymbol{r}\cos\theta^*. \qquad \text{(Eq 4)}$$

Here $\boldsymbol{r}$ is the average roughness ratio (actual area/projected area). As $\boldsymbol{r}$ is always ≥ 1, this means that if $\theta^* > 90°$, θ_m increases with increasing roughness; the contrary when $\theta^* < 90°$.

The triple line can also be "pinned" by the presence of surface heterogeneities. In order to override the grooves and ridges, that alter the local geometrical profile of the surface with an orientation of the contact plane different from the original reference one, the moving triple line should possess an additional energy. This requirement originates the appearance of "advancing" and "receding" contact angles (the difference between the two is called hysteresis). On the basis of energetic arguments (Ref 75, pp. 24-42, 113), it is possible to establish, inter alia, their maximum (advancing) and minimum (receding) values.

If the surface is plane, but chemically heterogeneous, i.e., surfaces formed by two different materials or different phases, but perfectly smooth, the macroscopic contact angle can be calculated using the Cassie-Baxter equation (Ref 114, 115):

$$\cos\theta_c = f_1\cos\theta_1 + f_2\cos\theta_2 \qquad \text{(Eq 5)}$$

where θ_1 and θ_2 represent the contact angles on fractions f_1 and f_2 of the total contact area, respectively.

4.2 Stoichiometry

The stoichiometry of the solid surface in contact with the liquid metal represents another important parameter in determining the wetting behavior of a particular solid-liquid system. Examples can be found in refs (Ref 116-124). Notwithstanding a certain dispersion of the experimental data, mainly due to the difficulty of characterizing the solid surface properties and the real experimental conditions, these studies seem to come to the conclusion that the higher the departure from stoichiometry in the solid surface the better its wettability by liquid metals. Often due to an enhanced metal-like electronic structure of the substrate. In particular, it has been shown that for non-stoichiometric titanium diborides (Ref 125) and titanium nitrides (Ref 118-120), wetting by liquid Cu and Au is better the higher the departure from the stoichiometric ratio. Other interesting systems are represented by metal/oxide samples.

The influence of stoichiometry on the wetting of stoichiometric (white) and of under-stoichiometric (black) zirconia by different metal melts was studied in a dedicated investigation (Ref 126). The results show that black zirconia is wetted by inert (Cu, Sn, Ag, Au, Pd, Pt, Cu-Ga, Pd-Rh) and by low active (Al, Cu-5Zr, (Cu-17.5 Ga)-10Ti) melts better than the white one, while reactive melts have contact angles on black and on white substrates close to each other.

The same problem has been also investigated by means of theoretical models. The wetting of sapphire by aluminum was simulated using the embedded atom method (EAM) and Coulomb potentials on a system of atoms with defined electronegativity (Ref 127). In the simulations of high-temperature wetting, the formation of an oxygen-deficient reaction layer between the liquid and the substrate was observed. This change in stoichiometry at the metal-ceramic interface may influence diffusivities in the surface of the ceramic and may therefore have an important effect on the kinetics of the evolution of surface features observed experimentally during reactive wetting.

The density functional theory (DFT) has also been used to investigate the role that the surface oxygen concentration on alumina has on the wetting by molten Ag, by evaluating the electronic properties of the system single constituents (nuclear and electronic charges), in principle "ab initio," without empirical assumptions on the model (Ref 62).

The section of an interface between sapphire (0001), center, and silver, on the two sides, resulting from the DFT calculation inspired by the experiments, is shown in Fig. 4. Additional oxygen atoms (red) have been inserted between the two silver layers that are closer to one of the Ag/sapphire interfaces, in different tetrahedral and octahedral positions. After relaxation of this oxygen-rich configuration, the work of adhesion increases considerably, in agreement with experimental data.

Similarly, another recent study (Ref 128) demonstrated that freshly sputtered ceria is hydrophilic due to excess surface oxygen (shown to have an O/Ce ratio of ≈3 and a water contact angle of ≈15°), which, when relaxed in a clean, ultra-high vacuum environment isolated from airborne contaminants, reaches close to stoichiometric O/Ce ratio and becomes hydrophobic (contact angle of ≈104°).

5. Wetting Studies

5.1 Transition Metal Diborides

Studies of the energetics of liquid metal/ceramic interfaces revealed that most of the iono-covalent ceramic/pure metal couples are "non-wetting systems" (with a contact angle $\theta > 90°$). This was verified mostly for oxide ceramics (Ref 41, 76, 106).

On the other hand, transition metal diborides have a metallic-like character, and, as already discussed, at their interface with a liquid metal a metallic bond should be established. This means that their wettability by liquid metals should be granted with equilibrium contact angles $\theta < 90°$. However, in many instances (Ref 133 and refs therein) a non-wetting behavior was found for these systems.

This means that a non-wettable layer should exist between the liquid metal and the diboride.

Thus, in order to achieve good wetting, means and procedures to "destroy" this barrier should be found. Diborides are intrinsically very reactive toward oxygen; in the case of XB_2 (X = Ti, Zr, Hf) the following reaction takes place:

$$XB_2(s) + 5/2\,O_2(g) \leftrightarrow XO_2(s) + B_2O_3(l) \qquad \text{(Eq 6)}$$

whose $\Delta G_{1500\ ^\circ C}$ is equal to −1190, −1337, −1340 kJ/mol for TiB_2, ZrB_2, HfB_2 respectively.

Moreover, diborides are nearly always either prepared by sintering procedures using specific aids to increase the final density or contain relevant quantities of a second phase designed to increase their oxidation resistance (usually SiC). In this case, in the presence of oxygen a surface layer can form, such as SiO_2, with a iono-covalent character.

Different mechanisms can be used to get rid of the "wetting barrier," linked to the large number of chemical reactions characterizing the diboride systems (Ref 129). They include:

(1) B_2O_3 removal.Despite the low oxygen partial pressure imposed to the system in the wetting experiments, it is possible that a very thin B_2O_3 layer (liquid at the test temperatures) could persist at the surface, for kinetic reasons. In this case, the following reaction can take place at the triple line

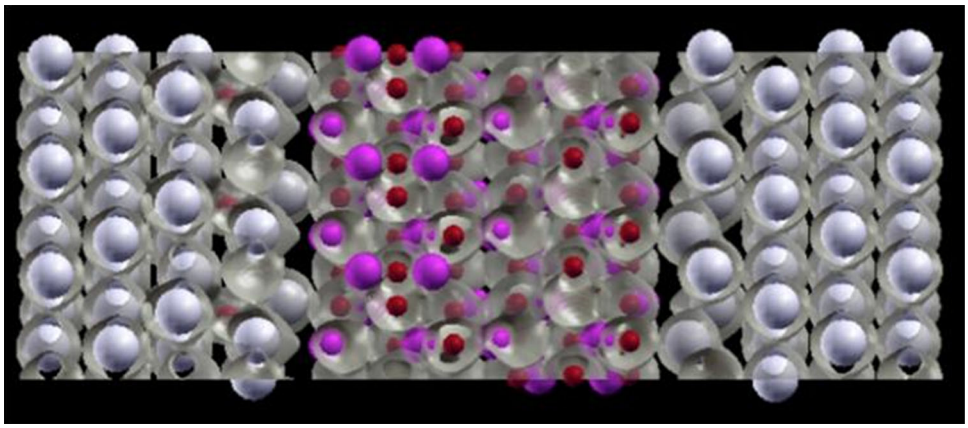

Fig. 4 Example of a Ag(111)/Al_2O_3 interface with an additional subsurface oxygen layer within the silver phase, after relaxation an additional oxygen atom appears between the last two interfacial layers of Ag(111) (left side). Courtesy D. Passerone, Empa, CH

$$2B + 2B_2O_3 = 3(B_2O_2). \quad \text{(Eq 7)}$$

This reaction has been studied (Ref 130) and the corresponding vapor pressure of the gaseous dimer $(BO)_2$, extrapolated to $T = 1520$ °C, results $P_{(BO)_2} \approx 6.1 \times 10^{-3}$ atm. Thus, while this result has to be taken with due caution, it clearly appears that, in the presence of boron dissolved into the liquid phase (as discussed below), reaction 7 can occur, and the gaseous B_2O_2 dimer can escape from the system allowing the drop to advance on the "bare" ceramic substrate, with a kinetics governed by this same reaction (Ref 131).

(2) Surface oxides reduction (e.g., SiO_2) by active metals (Ti, Zr, Cr…).The following reaction between the active metal AM and the SiO_2 could occur:

$$SiO_2(s) + 2AM(l) = 2AM - O + Si(l) \quad \text{(Eq 8)}$$

with the probable production of a sub-stoichiometric AM oxide, whose enhanced metallic character reduces the solid-liquid interfacial energy thus increasing wetting.

(3) Boride stoichiometry variation.As already mentioned, wetting is definitely affected by the ceramic substrate stoichiometry. Referring to the already cited case of TiB_2 (Ref 125, 132), the increased wetting effect was attributed partly to the variation in Boron content in the near-surface diboride layers and partly to the (very limited) dissolution of TiB_x into the liquid metal.

From a more general point of view, important improvements of the wettability of ceramic materials are obtained by adding "active metals" (such as Ti, Zr, Cr, Mo) to the liquid phase. At the interface, these "active" elements form intermediate products more readily wetted by the liquid alloy. As an example, the addition of Ti to Ag or Cu alloys involves the formation of Ti compounds (TiO, TiC, or TiN on oxides, carbides, and nitrides, respectively) at the metal-ceramic interface which, due to their more "metallic" character, are wetted better than the bulk ceramic.

Active metals, can also adsorb at the solid-liquid interface lowering the interfacial energy also affecting the spreading kinetics and consequently the final contact angle.

5.2 Recent Results

In our previous paper (Ref 133), we reviewed the work up to the year 2011. Therefore, in this paper, we will mainly discuss only what has been done thereafter. It should be noted that, despite the interest in the production and characterization of Ti, Zr, and Hf diborides, driven by their extremely attractive application potential, studies on their interactions with molten metals are still limited.

Among them, an investigation on the system Al/TiB_2 (Ref 134), of particular interest for the interaction with the electrodes in the aluminum industry, has shown that Al already starts wetting the TiB_2 substrate at 750 °C and that the wetting becomes better and better with increasing temperature. A final contact angle $\theta \ll 20°$ was found above 1000 °C after a few minutes. The experiments were performed by the "capillary purification" technique under high vacuum (Ref 135), so that the Al drop came into contact with the solid support only at the selected temperature, avoiding any contact reactions during the heating up period. Moreover, and this is extremely important for Al, the presence of an oxide layer on the drop surface was minimized by the "squeezing" process out of the capillary.

In addition, no extensive reactions between liquid Al and TiB_2 were found, although the presence of some AlTi and Al_4C_3 particles were found at the solid-liquid interface, witnessing a limited dissolution of the solid support. However, beginning from 1000 °C, liquid Al penetrates the TiB_2 substrates by filling pores and grain boundaries (reaching $\approx$ 250 μm after 15 min at 1400 °C).

The NiAl-MeB_2 (Me = Zr, Ti, Cr) system was studied at 1650 °C in order to understand the interactions occurring during the fabrication of NiAl-based composites reinforced by diborides particles (Ref 136). The wetting tests resulted in low contact angles, with $\theta = 11°$, 20°, 0° for molten NiAl in contact, respectively, with ZrB_2,TiB_2, and CrB_2. In particular, a stable wetting angle of 20° in the NiAl-ZrB_2 system was recorded after 7 min. In the case of the NiAl-TiB_2 system, the contact angle of 11° was reached in 10 min. The best wetting was observed in the case of the NiAl-CrB_2 system. During the first 3 min, the angle reaches 22°, and after 6 min the spreading of the drop was nearly complete with a final contact angle close to zero. In both ZrB_2 and TiB_2 systems, no new phases were found at the interface, while a deep penetration along the grain boundaries of the ceramic matrix was observed. An interesting result is that NiAl does not seem to dissolve the underlying Zr or Ti diboride substrates, although it penetrates along the solid grain boundaries. These results are in agreement with a subsequent study on the NiAl system in contact with (Ti-Cr)B_2-AlN composites (Ref 137), where a very good wetting was found in the temperature range 1550-1600 °C with final contact angles below 10° without strong dissolution of the substrate. On the contrary, NiAl was found to interact with "pure" CrB_2 penetrating deeply into the solid substrate, and reacting with it giving rise to various new phases and intermetallic compounds.

Strong interactions were found when studying the behavior of molten Cr in contact with Ti, Zr, and W borides (Ref 138) in the temperature range $1300 < T < 1950$ °C. During heating, a liquid phase formed at the contact area at around $T = 1600$ °C (contact melting). The contact angle between the liquid and titanium diboride was initially 70° to 75° decreasing gradually to 40° to 45° during holding. During further holding at 1600 °C, the drop partially spread over the sample and then solidified.

Similar behavior was found with W_2B_5 and ZrB_2, the only differences being that the liquid phase formed and spreading proceeded at higher temperatures ($T \approx 1700$ °C for W_2B_5 and $T \approx 1850$ °C for ZrB_2) with final contact angles $\theta = 10°$, 12°, 45° at $T \approx 1950$ °C for the Ti, W, and Zr borides respectively.

Thus, Cr seems to enter into strong interaction with the transition metals diborides, giving rise to dissolution and reaction phenomena at the solid-liquid interfaces.

These results are in agreement with a series of studies on the interaction of Ni and Ni alloys with Ti, Zr, and Hf diborides, undertaken by this Group in the last 15 years (Ref 43, 103, 139-142, 151, 152). It has been shown that pure Ni wets HfB_2 and ZrB_2 very well. However, strong reactivity and dissolution of the ceramics were detected. Further studies on the ternary phase diagrams for the B-Ni-X (X = Ti, Zr, Hf) systems carried out using the CALPHAD method (Ref 140) demonstrated that reactivity can be reduced or even suppressed by proper additions of B to Ni (Ref 103, 141). Wetting tests performed using the suggestions deriving from the CALPHAD modeling,

confirmed the strong reduction of reactivity by means of the Ni alloy saturation.

The sessile-drop experiments were made using three different Ni-B compositions as starting alloys, namely: pure Ni, Ni plus 17 at.% B (NiB17) (eutectic composition), and Ni plus 50 at.% B (NiB50) slightly hypereutectic (Ref 103). The experiments have been done at 1520 °C; moreover, some additional tests have been made at 1200 and 1130 °C to clarify the role of the ternary $Hf_2Ni_{21}B_6$ compound (which melts at 1230 °C) in the behavior of the Ni-HfB_2 system in this specific temperature range.

The behavior of contact angles versus time for the three Ni alloys in contact with the HfB_2 substrate at 1520 °C is shown in Fig. 5.

The cross sections of the wetting samples in Fig. 6 show that dissolution of the ceramic material occurred for pure Ni and for the NiB17alloy, while it almost disappeared for the NiB50 alloy.

Two results must be underlined: in all cases, the largest part of the solid-liquid interactions occurs during the first minute of contact, both in the cases where strong dissolution of the substrate takes place, and in the case of the NiB50 alloy where no dissolution at all was found. Moreover, in the cases with dissolution, the contact angles remain nearly constant for the first few minutes of contact, while in the case of wetting without dissolution the contact angles keep decreasing for a long time and does not seem to have reached an equilibrium value even after 10 min.

As shown in Fig. 6, the strong interaction between pure Ni and the ceramic substrate, leads to penetration of the newly formed liquid Ni alloy between the HfB_2 grains and to the formation of the sigmoidal shape of the solid-liquid interface already described. Upon melting NiB17 dissolves a much smaller amount of HfB_2 than in the case of pure Ni. The sigmoidal shape of the interface is retained (Fig. 6), suggesting the same interaction mechanism as in the previous case. Similarly, the molten Ni alloy penetrates along the grain boundaries of the ceramic substrate. A noticeable crystallization of the HfB_2 grains is also found at the solid-liquid interface.

The bulk-solidified drop shows a well-developed eutectic structure (Fig. 7), where one of the two phases is essentially formed by the ternary $Hf_2Ni_{21}B_6$ compound and the other one has a composition close to Ni_3B. Indeed, the calculated pseudo-binary section (Fig. 8) foresees the presence of all of these phases down to 212 °C: this configuration can be considered to remain frozen during the non-equilibrium cooling. At variance with the pure-Ni case, it is also worth noting that HfB_2 crystallization is practically absent in the liquid phase, due to the fact that a smaller amount of HfB_2 is dissolved at the test

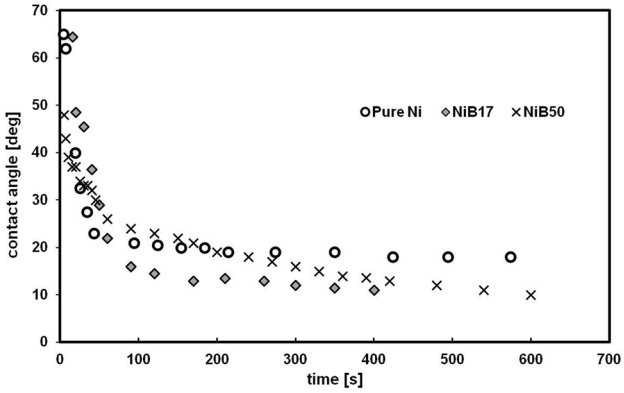

Fig. 5 Contact angles versus time of Ni-B alloys on HfB_2 at 1520 °C (Ref 43)

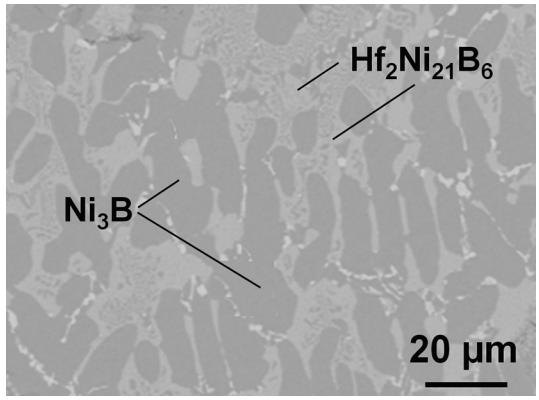

Fig. 7 SEM-BSE images of the microstructure of the NiB17/HfB_2 system showing the eutectic structure containing Ni_3B (dark) and $Hf_2Ni_{21}B_6$ phases (light)

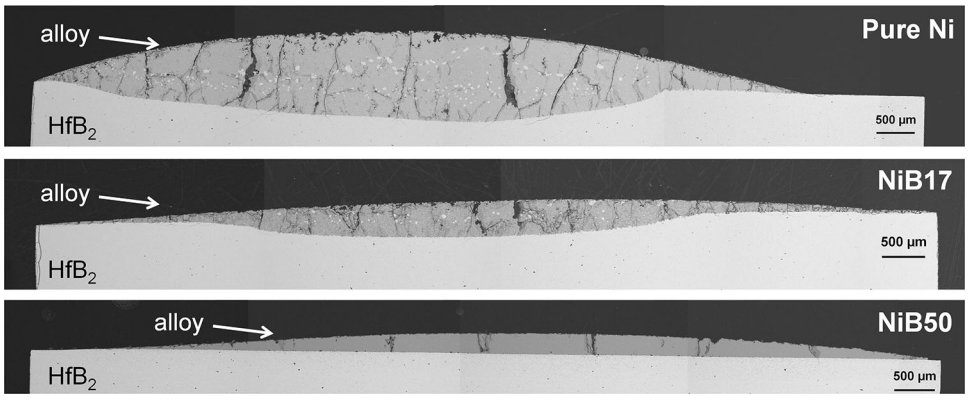

Fig. 6 Cross sections of samples after high-temperature interaction with HfB_2 (scanning electron microscope-backscattered electrons, SEM-BSE)

temperature compared to the pure-Ni case, and that the dissolved part is used to form the large amount of ternary compound.

The NiB50 alloy spreads over the HfB_2 substrate a little bit slower than pure Ni and the NiB17 alloy (Fig. 5) and, in 10 min, it does not reach a final equilibrium value, even if θ is quite small ($\theta < 10°$). The interface is sharp and planar, with no detectable dissolution of the substrate into the liquid phase. As shown in Fig. 9 the isothermal section shows that, at $T = 1500$ °C, the NiB50-HfB_2 line crosses the liquidus line at $X_{Hf} \approx 0.03$ (point A2), a concentration that drops to nearly zero already at 1130 °C. The crystallization of HfB_2 at the interface is consistently much smaller than in the other cases and no Hf can be detected in the liquid, which retains an eutectic structure after solidification formed of Ni_2B and Ni_4B_3 with particles of pure boron precipitated at the metal/ceramic interface (Fig. 10). However, a Ni-rich penetration zone, about 80 mm thick, is clearly visible in the ceramic phase beneath the drop.

Parallel tests have also been carried out at 1200 and 1130 °C, chosen as being above and below the melting point of the intermetallic compound Ni_3B, but also just close to the melting point of the ternary $Hf_2Ni_{21}B_6$ compound ($T = 1230$ °C). The NiB17 alloy, corresponding to the eutectic composition, melts at $T = 1093$ °C and could offer a good choice as brazing alloy, in particular using the transient liquid phase bonding process (Ref 37).

The tests at 1200 °C showed a good wettability of the molten phase, which reached a stationary contact angle of $\theta \approx 37°$ in about 5 min. The shape of the molten drop remained smooth for all the holding times.

With reference to Fig. 11, the NiB17 alloy melts and starts dissolving (point B) an important amount of HfB_2 until the equilibrium composition of point C is reached. It is worth noting that the intermetallic ternary compound $Hf_2Ni_{21}B_6$ can form at around this temperature, but not if the boron content of the starting alloy in contact with HfB_2 is above ≅ 15 at.%.

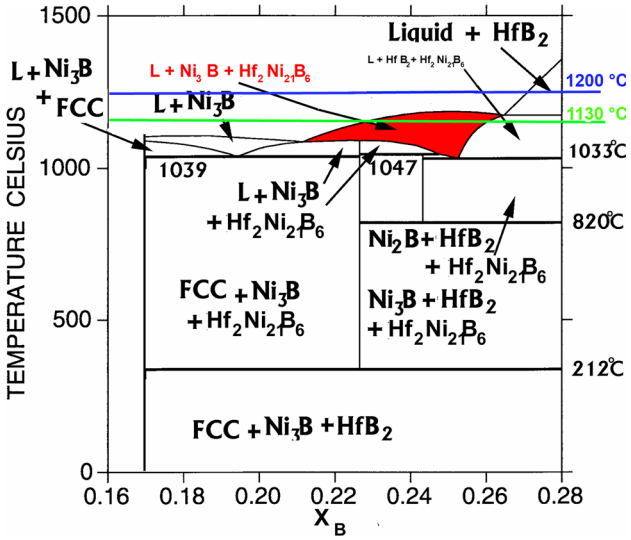

Fig. 8 Pseudo-binary section of NiB17-HfB_2 phase diagram

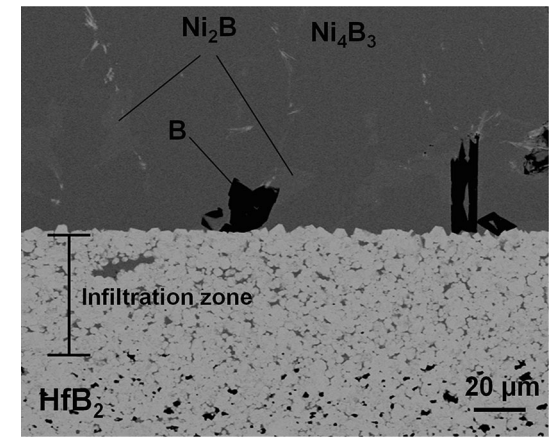

Fig. 10 Section of the NiB50 drop on HfB_2, treated at 1520 °C, showing the internal structure with Ni_4B_3 (dark gray), Ni_2B (light) and B (black), and the alloy penetration along grain boundaries and pores of the HfB_2 (SEM-BSE picture)

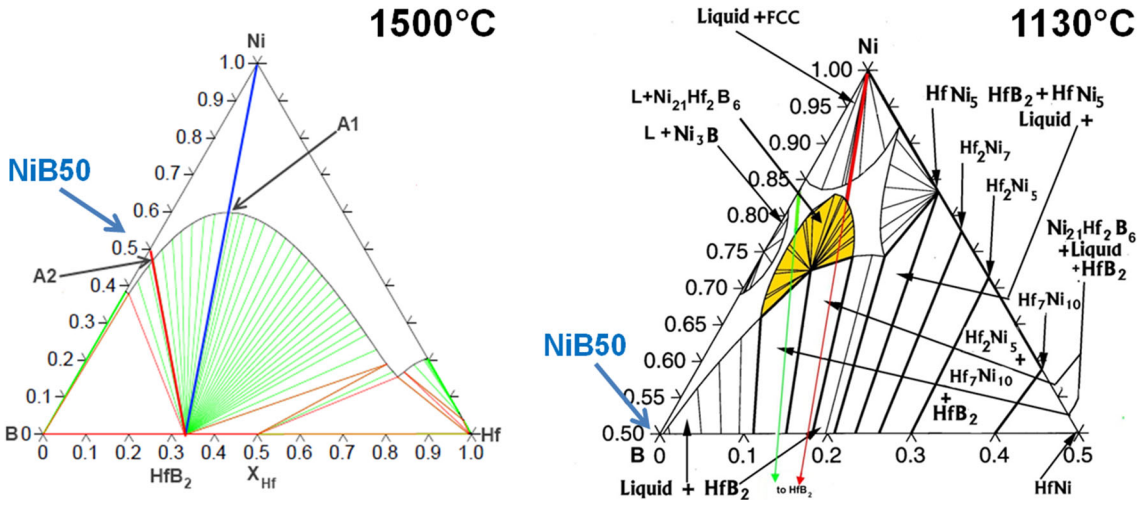

Fig. 9 Isothermal sections of Ni-B-Hf phase diagram at 1500 °C and at 1130 °C

The micrographs shown in Fig. 12 show that the ternary $Hf_2Ni_{21}B_6$ (light gray phase) and binary (dark gray) formed during solidification and the liquid alloy deeply penetrated the sintered substrate.

At $T = 1130$ °C, after melting, the drop forms regularly and spreads on the HfB_2 surface for about 3 to 4 min. But after this initial period, the drop profile loses its regular shape and some "solid"' inclusions appear, until the whole profile is perturbed and no liquid phases seem to be left (Fig. 13). These phenomena will be discussed more in detail in the next section.

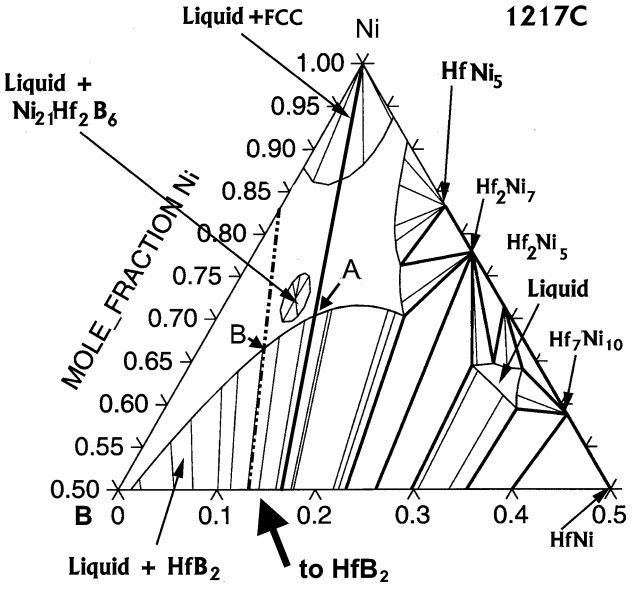

Fig. 11 Calculated B-Ni-Hf at 1217 °C (Ni-rich corner)

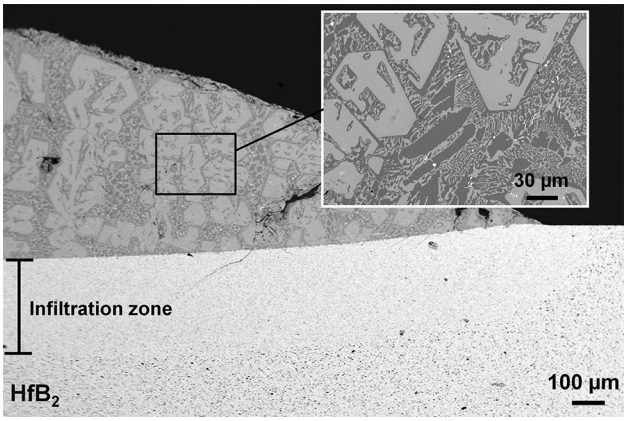

Fig. 12 Interface structure of the NiB17/HfB_2 specimen treated at 1200 °C

A nearly parallel study was carried out for the Ni alloys/ZrB_2 system (Ref 139). The wetting of ZrB_2 by Ni and two binary Ni-B alloys was evaluated by means of the sessile-drop method at 1500 and 1200 °C.

The results, summarized in Table 1, show that a condition of wetting ($\theta < 90°$) was achieved. At 1500 °C, pure Ni wets ZrB_2 according to the spreading kinetics shown in Fig. 14.

Three steps can be recognized: (a) a first spreading phase immediately after the melting of the metal; (b) a stationary stage lasting about 450 s with a constant contact angle $\theta \approx 23°$; and (c) a further spreading phase with a final contact angle of less than 10°. For the NiB17 alloy, a similar spreading kinetics was reported, and the final contact angle was less than 10° as well.

For the NiB50 alloy, after the spreading process, taking place in about 25 s, no further evolution occurred, and the final contact angle was 30°.

The cross sections of the three pairs, tested at 1500 °C, namely Ni/ZrB_2, NiB17/ZrB_2, and NiB50/ZrB_2, are shown in Fig. 15. A remarkable substrate dissolution is clearly visible at the solid/liquid interface in the Ni/ZrB_2 cross section, and the sigmoidal profile of the interface is formed. The same phenomenon, even if less pronounced, can be observed in the case of NiB17, while it is suppressed for NiB50.

Table 1 Summary of the final contact angles (deg ± 2°)

	Pure Ni	NiB17	NiB50
1500 °C	< 10°	< 10°	30°
1300 °C	…	21°	58°

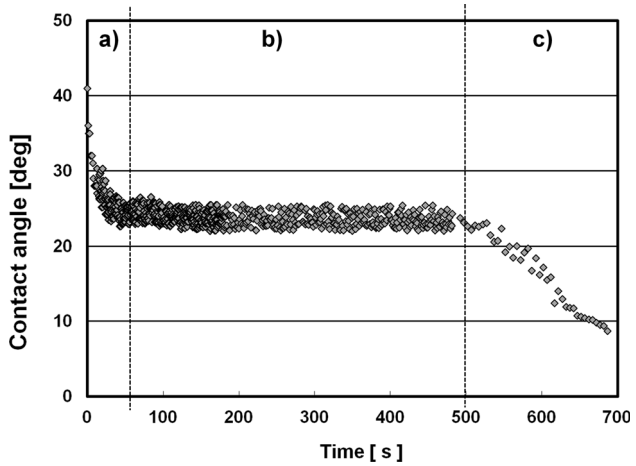

Fig. 14 Contact angle versus time for a liquid Ni drop in contact with ZrB_2

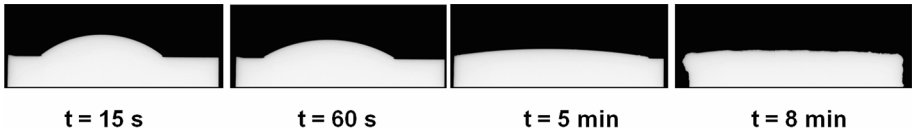

Fig. 13 Wetting sequence of NiB17 on HfB_2 at 1130 °C

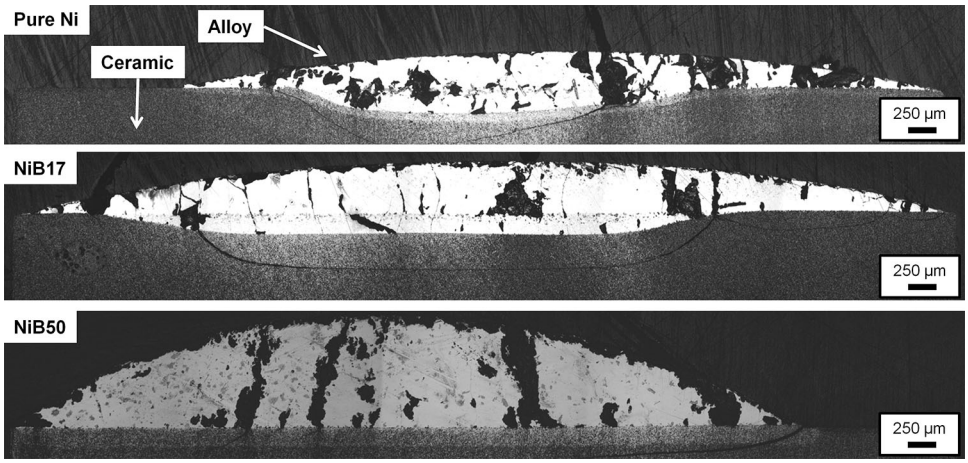

Fig. 15 Cross sections of the Ni/ZrB_2, NiB17/ZrB_2, and NiB50/ZrB_2 samples tested at 1500 °C (optical microscope images) (re-drawn from Ref 139)

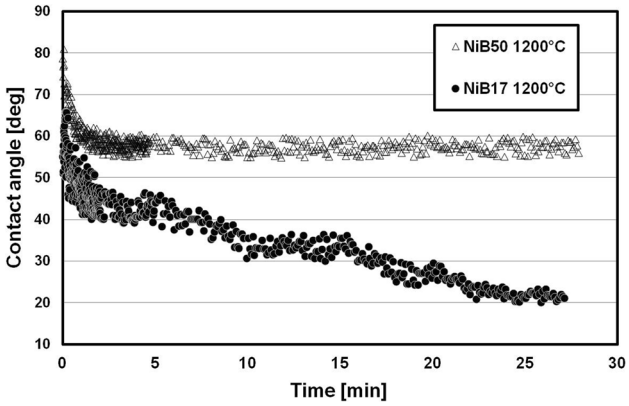

Fig. 16 Spreading kinetics of Ni-B alloys on ZrB_2 at 1200 °C

Wetting tests have also been performed at 1200 °C with NiB17 and NiB50; the final contact angles were 21° and 58°, respectively.

The NiB17 alloy wetted the ZrB_2 substrate with a spreading kinetics (Fig. 16) that did not stop even after 25 min from the beginning of the test. At the same time, the drop base diameter increases, and the height decreases.

On the contrary, the spreading of the molten NiB50 alloy takes place in 200 s, and afterward the contact angles do not show any further variation. Cross sections of the NiB17/ZrB_2 and NiB50/ZrB_2 pairs are shown in Fig. 17. While the former shows a sigmoidal shape, meaning that an interaction between alloy and ceramics occurs, the resulting NiB50/ceramic interface is macroscopically planar.

The EDS analyses performed on the NiB17/ZrB_2 wetting couple show the formation of an eutectic structure of the metallic phase for the NiB17 alloy with formation of the compound $Zr_2Ni_{21}B_6$.

The NiB50 alloy showed the highest final contact angles toward ZrB_2: 30° and 58° at 1500 and 1200 °C, respectively.

The tests made at 1130 °C had a strikingly different behavior.

Similarly to what was found for the NiB17-HfB_2 system, in the NiB17/ZrB_2 system, at 1130 and 1110 °C, the wetting phenomenon starts with a rapid decrease of the contact angle associated to a reduction of the drop height and to an increase of the drop diameter (part a of Fig. 18). However, after about 11 min from the beginning of the experiment, a change in the drop shape occurs caused by a partial solidification of the alloy (part b). A few minutes later (at 1130 °C), a further melting takes place and the drop remains in the liquid state until the end of the test (part c).

The spreading kinetics, reported in Fig. 18 for the sample held at 1130 °C, shows that the contact angle just before the solidification is ≈20°, similar to the samples tested at 1200 °C. It then decreases to values lower than 10° after the second melting. Measurements of the drop dimensions of these specimens reveal three distinct trends that can be associated to different stages of the experiment, indicated in Fig. 18: (a) After the initial rapid spreading, lasting ≈ 30 s, the drop height gradually decreases, while the diameter increases, meaning that the liquid drop spreads over the ceramic, (b) the diameter decreases during solidification, and (c), similar to point (a), the drop height decreases again and the diameter increases, as a second spreading takes place after remelting.

6. Interpretation of Wetting Results by Phase Diagrams

As presented in section 5, the combination between the complex wetting and reactivity results and the thermodynamic interpretation through multi-component phase diagrams are one of the best ways to:

predict the interfacial behavior of metal/ceramic systems (dissolution, reactivity…)
assist the formulation of new alloy compositions
interpret the liquid/solid phenomena
interpret wetting and microstructural results.

However, most of the phase diagrams relevant to the interactions between Group 4 diborides and transition metals, e.g., nickel, were poorly known or not known at all. As a consequence, an effort has been made to implement a CALPHAD thermodynamic database

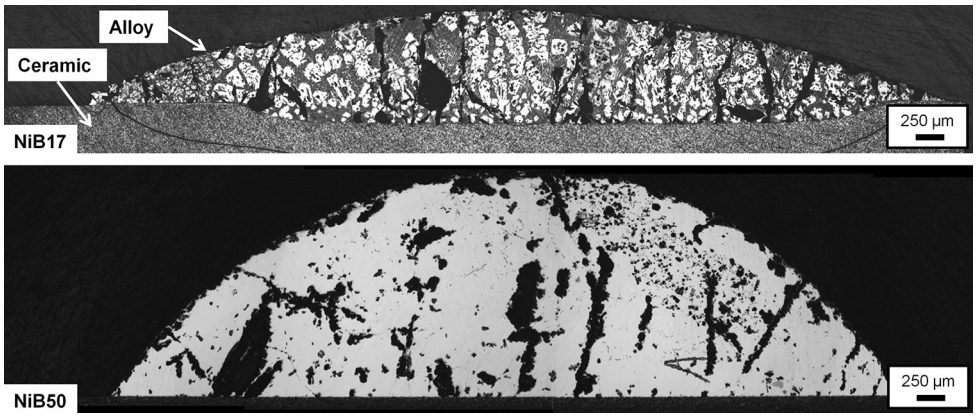

Fig. 17 Cross sections of the NiB17/ZrB_2 and NiB50/ZrB_2 specimens treated at 1130 °C (optical microscope images) (re-drawn from Ref 139)

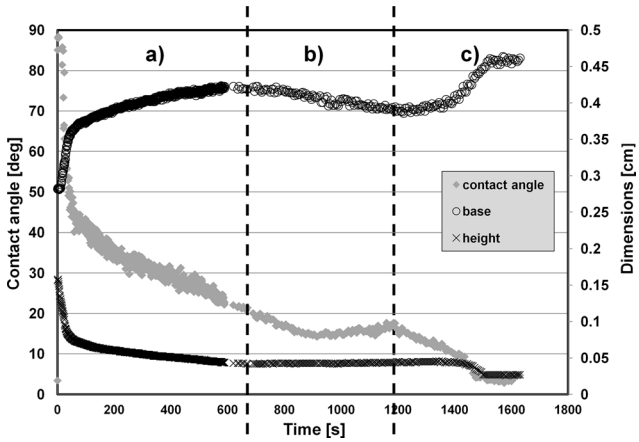

Fig. 18 NiB17/ZrB_2 spreading kinetics at 1130 °C (re-drawn from Ref 141)

for phase diagram calculations in the quinary system B-Hf-Ni-Ti-Zr (Ref 132, 141). Thermodynamic models for 30 different phases have been determined and interaction parameters for all the 10 binary and 10 ternary sub-systems have been included. Several ternary systems (B-Hf-Ni, B-Ni-Ti, B-Ni-Zr, B-Hf-Zr, B-Ti-Zr, Hf-Ni-Ti, Hf-Ni-Zr, Hf-Ti-Zr, Ni-Ti-Zr) have been completely assessed or re-assessed. As a result, ternary isothermal sections at the various test temperatures can be obtained, with all the binary phases, the ternary liquid as well as the existence field of the ternary $X_2Ni_{21}B_6$ "tau" solid phase (X = Ti, Zr, Hf).

In addition, isopleths of the equilibrium transformations of the Ni-X/diborides pairs are also available, making it possible to interpret the solidification structures.

The phase diagrams relevant to the study of high-temperature interactions between Ni and early-transition metal diborides (TiB_2, ZrB_2 and HfB_2) are very similar. For example, the isothermal sections at 1500 °C of the B-Ni-Ti and B-Ni-Zr systems (Fig. 19) could be compared to the B-Hf-Ni one presented in Fig. 9. Therefore, as shown before, for all these systems, when the molten Ni-B alloys are brought into contact with XB_2 at a certain temperature, an equilibrium condition is established between the two phases, which can be followed on the corresponding isothermal section.

As a further example (Fig. 20), pure Ni, when placed in contact with ZrB_2, melts at a temperature (about 1100 °C) well below its melting point (1453 °C), giving rise to a ternary liquid phase due to the dissolution of ZrB_2 as described in section 5.

The isothermal section at 1500 °C of the ternary diagram (Fig. 19, right) also shows that, at the same temperature, the dissolution of the boride is greatly reduced and almost disappears if a Ni-B alloy with $X_B > 0.50$ is placed in contact with ZrB_2. Indeed, pure Ni in contact with ZrB_2 enters a biphasic equilibrium formed by a solid (ZrB_2) and a liquid phase with composition indicated by point α. An increased amount of B in the alloy causes a reduction in the ZrB_2 dissolution and a variation of the liquid-phase composition, which follows the liquidus line from point α through point β to γ for Ni, NiB17, and NiB50, respectively. The reduced substrate dissolution with increasing B content explains the gradual disappearance of the sigmoidal shape of the interface previously described.

On lowering the temperature, the ZrB_2/liquid biphasic region of the Ni-ZrB_2 isopleth widens, the concentration of Ni in the liquid increases, and, at the same time, the crystallization of a certain amount of ZrB_2 takes place. The extent of this phenomenon decreases from Ni to NiB17 to NiB50, as the composition of the liquidus at 1500 °C becomes poorer in Ni (points β and γ, respectively).

For these reasons, remarkable amounts of crystallized ZrB_2 can be found in the solidified Ni drop, while smaller amounts are present in NiB17 and NiB50. According to the phase diagram, at 1500 °C a triphasic region exists close to the boron corner, where B, ZrB_2, and a liquid phase coexist. Indeed, as shown by the NiB50-ZrB_2 isopleth (Fig. 21), by lowering the temperature, this region widens reaching a narrow region of coexistence (liquid + B + ZrB_2) at about 1000 °C: for this reason, boron crystals can be found in the NiB50-solidified drop similarly to what was observed for the NiB50-HfB_2 system (Fig. 10). The same isopleth shows that, as revealed by microanalysis, the $Zr_2Ni_{21}B_6$ compound cannot exist and that the solidification leads to a Ni-B alloy, boron crystals and ZrB_2.

Moreover, wetting experiments can help to validate phase diagrams calculations.

The phenomena occurring at 1130 °C in both the cases of HfB_2 and ZrB_2 substrates, described in the previous paragraphs, can be successfully interpreted on the basis of the ternary computed phase diagrams (Ref 141, 142). The isothermal section at 1130 °C is reported in Fig. 22; the dotted line joining NiB17 to ZrB_2 connects the compositions of the starting materials and indicates how the global composition of the drop

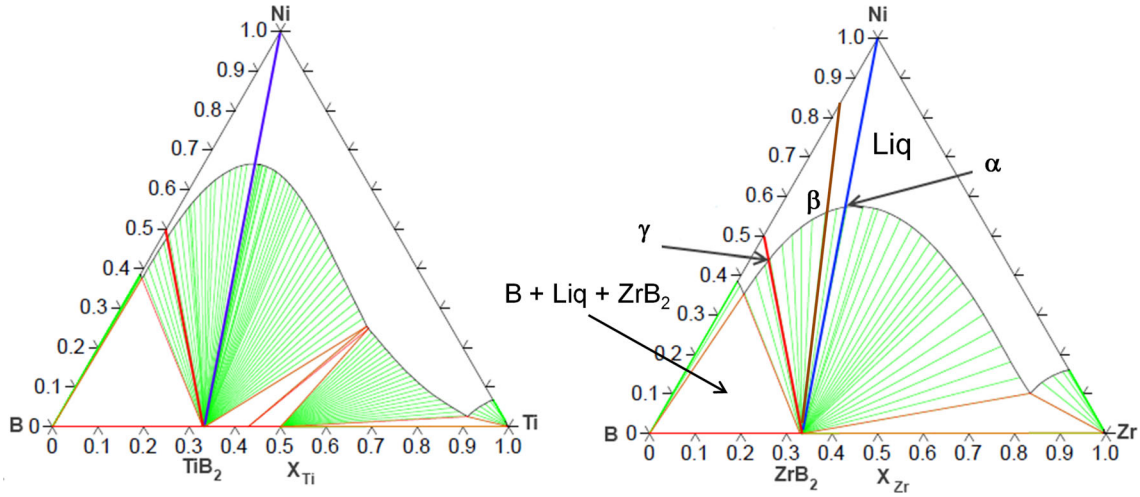

Fig. 19 Calculated ternary phase diagrams, isothermal sections at 1500 °C. Left: B-Ni-Ti system; right: B-Ni-Zr system (from Ref 133, with permission)

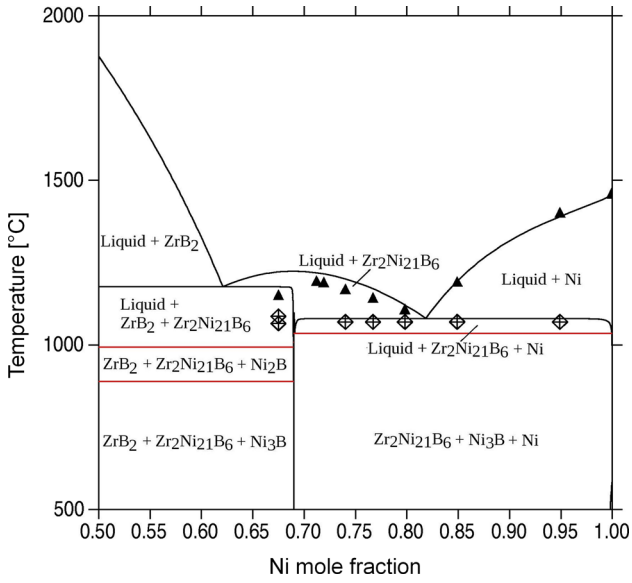

Fig. 20 The pure Ni-ZrB_2 vertical section

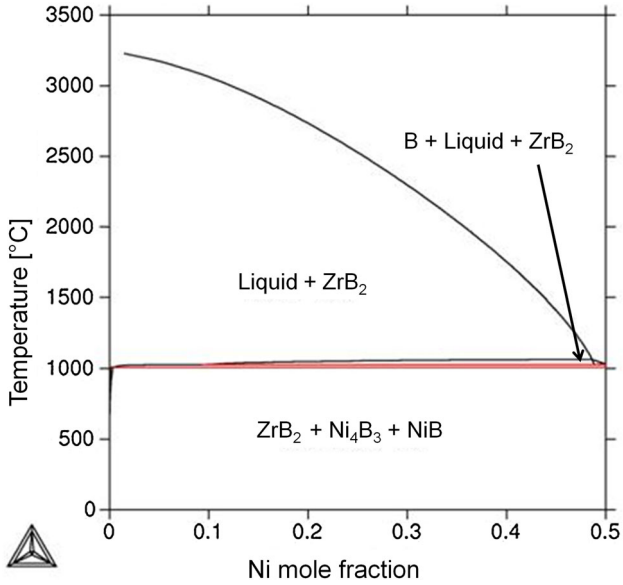

Fig. 21 Vertical section along the NiB50-ZrB2 line of the Ni-B-Zr ternary diagram (from Ref 139, with permission)

changes while dissolving ZrB_2. It crosses the liquid + $Zr_2Ni_{21}B_6$ two-phase field (labeled with A). This biphasic field shrinks with increasing temperature and disappears at the melting temperature of the ternary compound (1186 °C < T_m < 1196 °C). However, the area of the A region widens with lowering temperature and, at T = 1124 °C, it collides with the (Ni_3B + liquid) two-phase field, so that a (liquid + $Zr_2Ni_{21}B6$ + Ni_3B) three-phase region appears. The A region, which is also present in the Ni-B-Hf and in the Ni-B-Ti phase diagrams (Ref 143), although at slightly different temperatures, is responsible for the occurrence of the liquid-solid-liquid transition described.

When in fact the NiB17 alloy is put in contact with ZrB_2 at temperatures ranging between 1110 and 1130 °C, due to the gradual dissolution of ZrB_2, the composition of the liquid drop changes with time along the dotted line until it reaches saturation (point B). As the A region is entered, the reprecipitation of $Zr_2Ni_{21}B_6$ starts, until the global composition lies inside the (liquid + $Zr_2Ni_{21}B_6$) two-phase field. The complete remelting of the drop explains why no $Zr_2Ni_{21}B_6$ layer can be found at the metal/substrate interface.

7. Joining

The interfacial phenomena discussed in the previous sections are very relevant for the design of reliable metal-ceramic brazing procedure. Indeed, the use of a liquid metal phase as the means to join materials of such different structures and properties, represents a challenge aimed at minimizing and controlling the dissolution phenomena, the reactions and the subsequent solidification transformations that determine the final resistance of the joint structure.

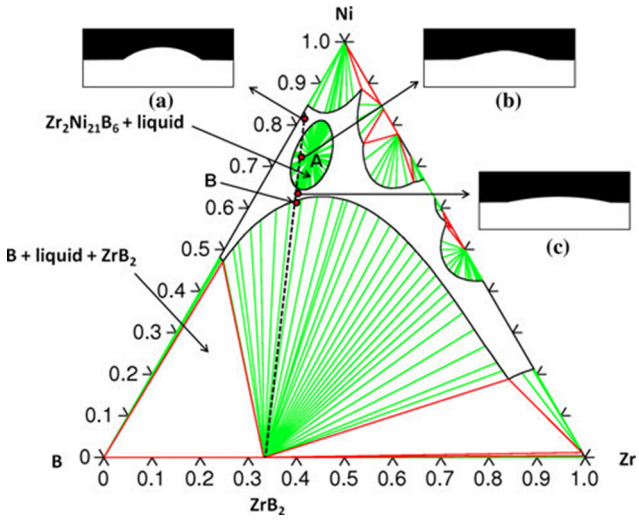

Fig. 22 Isothermal section at 1130 °C of the Ni-Zr-B system. The dotted line joining NiB17 to ZrB_2 shows the system under study. The insets refer to the wetting test at different stages: (a) initial melting, (b) isothermal solidification, (c) remelting of the drop and further wetting (from Ref 141, with permission)

In recent years the increasing interest in ultra-high-temperature ceramics has led to a number of new studies specifically related to joining processes, mainly by means of brazing procedures.

It should first of all be noted that these studies refer to composite ceramic materials, i.e., materials where a second component has been added to the main ceramic body to improve its oxidation resistance and/or its mechanical properties. This means that the possible interactions between the liquid filler alloy and the ceramic itself can be much more complex than those studied with reference to the "pure" matrix.

Just referring to recent studies involving diboride ceramics, the joining of ZrB_2-SiC to various metals has attracted great interest. In these cases, SiC is added to the ZrB_2 matrix, in general up to 20 vol.%, in order to make this composite more resistant to oxidation and to mechanical loads in highly aggressive environments.

The joining of ZrB_2-SiC to metallic systems was studied between the years 2007 and 2010 by Asthana and Singh and have been reviewed in (Ref 23, 134). Recently (Ref 143), the same Authors demonstrated the feasibility of joining ZrB_2-SiC (fibers, particles) to Ti and Inconel-625 by using amorphous Ti-brazes at $T < 850$ °C as a filler. The obtained joint regions were sound and well-bonded, although a few cracks close to the UHTCs have been found; in particular, cracking was found to be more severe in UHTC/Inconel than in UHTC/Ti joints (larger residual stress in the former), suggesting the need to implement specific stress-mitigating metallic interlayers. Nevertheless, the use of the amorphous Ti-brazes gave rise to much more limited chemical interactions compared to the joints obtained with the Pd-Co and Pd-Ni brazes examined in the previous studies (Ref 144, 145). In agreement with that, we can add that some of our still unpublished studies have shown that Pd-based alloys lead to an increased boride dissolution.

Saito et al. (Ref 146) reported on the wetting behavior of molten Ni-Nb alloys used for TLP bonding of HfB_2 + $MoSi_2$ at 1500 °C. Ni-Nb alloys wet well the HfB_2-$MoSi_2$, with substantial interfacial reaction. It was confirmed that the 40 at.% Nb addition to Ni significantly reduced the dissolution of HfB_2 composite. The result of the TLP bonding has shown that the interlayer and composite were well bonded, with no cracks in the interfacial region. The use of sintering aids had a significant modifying effect on the wetting and joint microstructure.

Other recent works report about the joining of diboride ceramics to themselves or to metals exploiting the well-known beneficial effect of Ti to adhesion and mechanical properties (Ref 147, 148). Joining procedures were also pursued through spark plasma joining (Ref 149) or by using Ni foams as a joining interlayer (Ref 150).

In the same period of time our group continued its work aimed at extending the studies about wettability of transition metals diborides to joining these diborides to themselves and to Ti alloys using Ag-Cu as well as Ni-B-based alloys (Ref 151, 152).

In the case of studies on wetting and brazing of ZrB_2 and ZrB_2-SiC to Ti6Al4V by Ag-Cu based alloys, Ag-Ti, pure Cu, and Cu-Ti interlayers have been tested, in order to achieve joints that could work in aggressive environments at temperatures around 800 to 850 °C for short times.

It has been shown that Cu wets pure ZrB_2 better than Ag, reaching a contact angle $\theta = 72°$ at 1150 °C. A slightly higher contact angle $\theta = 80°$ was obtained on the ZrB_2-SiC composite, while for Ag a non-wetting situation was found ($\theta = 97°$ at 1023 °C). The wetting of diborides ceramics by these pure metals depends strongly on the characteristics of the surface in contact with the liquid metal which, in turn, depend on the experimental conditions (temperature, atmosphere) and on the chemistry of the ceramic (presence of SiC or sintering aids). The introduction of Ti, which segregates at the S/L interface improves the wetting behavior substantially: for Ag-9 at.% Ti, $\theta = 10°$ was found at 1023 °C, while for Cu-22 at.% Ti a contact angle $\theta = 19°$ was found at 950 °C.

Tests made on ZrB_2–SiC/Ti6Al4V joints, obtained by active metal brazing using the Ag-Ti alloy, showed crack-free microstructures with a good final mechanical behavior with an average shear strength of 79 MPa (Fig. 23a). On the other hand, when put into contact with the Ti alloy, pure Cu forms a liquid phase even at temperatures below its melting point (contact melting). This liquid phase evolves to Ti-Cu intermetallic compounds or to Cu dissolved into Ti depending on the process temperature and, as a consequence, on diffusion processes, where the Ti6Al4V phase has the role of Ti source for the filler alloy. Joining tests made at 950 and 1050 °C using pure Cu sandwiched between ZrB_2-SiC and Ti6Al4V demonstrated the possibility of obtaining good wetting and good adhesion of the filler alloy to both substrates, with an evenly distributed filler alloy layer resulting in sound joints. Keeping Ti to diffuse into the liquid Cu phase can lead to the isothermal solidification of the filler alloy, laying down the basis for the design of a joining process by the TLPB technique.

The brazing of ZrB_2 and ZrB_2-SiC to Ti6Al4V has also been studied at higher temperatures using Ni alloys at 1100 °C as filler metals (Ref 152). The results of the wetting tests and the analysis of phase diagrams reported in the previous sections, have been used for choosing the processing parameters (alloy composition, holding time, temperature) in the production of the joints.

In particular, a slurry coating of Ni-B50 in form of powder was used as a brazing filler for the ZrB_2-SiC/Ti6Al4V system. It has been confirmed that this brazing medium, wets the adjoining surfaces from the very beginning of the process,

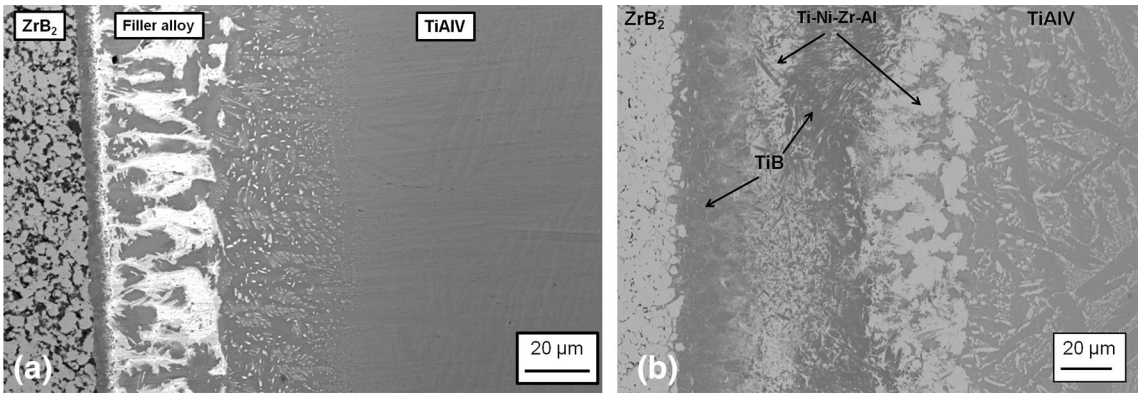

Fig. 23 Cross sections of ZrB_2-SiC/Ti6Al4V joints obtained by (a) Ag-Ti or (b) NiB50 interlayers (SEM-BSE images) (from Ref 151, 152, with permission)

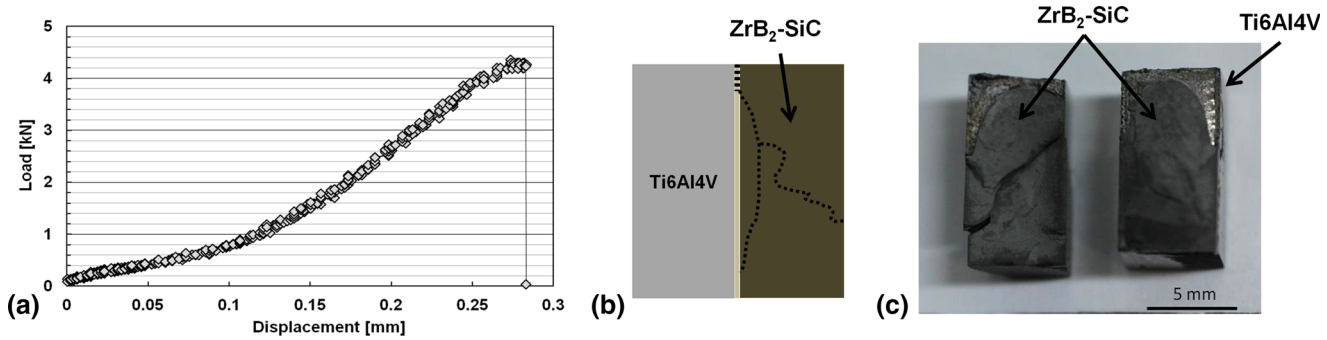

Fig. 24 (a) Load-displacement curve for a shear test; (b) sketch of the way of rupture of samples and (c) picture of a sample after failure (re-drawn from Ref 152)

assuring an intimate contact by effect of the capillary pressure, leading to a good adhesion of the filler alloy along the metal-ceramic interface. A complex multilayer structure, with a thickness of about 100 μm, appeared at the interface between the two materials as a result of the interdiffusion phenomena and of the nucleation of new phases at the testing temperature or during cooling. Microstructural examination showed that Ti diffused from the Ti6Al4 V alloy toward the ceramic surface, leading to a very complex microstructure (Fig. 23b). The region closest to ZrB_2-SiC contains TiB whiskers interspersed in a $(Ti, Zr)_2Si$ + (Ti-Zr-Si) solid solution. On the Ti6Al4 V side, the (TiNiZrAl)-based quaternary alloy is mixed to Ti6Al4 V, while relevant amounts of Ni are diffused into the Ti6Al4 V. Interfacial layers were reputed to have an important role in accommodating the thermal mismatch between the adjoining materials. In particular, TiB has a CTE (8.6×10^{-6} °C^{-1}) intermediate between that of ZrB_2 ceramics and TiAlV.

A good mechanical performance was obtained for these ZrB_2-SiC/NiB50/Ti6Al4 V joints. The load-displacement curve (Fig. 24a) obtained in shear tests shows that the samples are deformed elastically with a small plastic deformation before final rupture which increases the total fracture energy. The shear strength, averaged over 3 samples, was 74 ± 16 MPa. Post-mortem visual observation showed that the rupture occurred along the ceramic part (Fig. 24b, c) indicating that the joint withstands mechanical loading better than the ceramic itself.

From these results we can summarize that three specific elements contribute to providing good final joints: (a) the suppression of the dissolution of the ceramic phase; (b) the formation of a continuous multilayer interfacial structure as a result of the good wetting conditions and of diffusion phenomena; and (c) the key role played by active elements such as Ti: during the process, Ti enriches the liquid phase improving the wetting, segregating at the metal-ceramic interface and forming compounds (e.g., TiB) with an increased metallic character. In specific cases, these compounds also contribute to adjust the CTE mismatch between ZrB_2 and Ti6Al4V.

8. Conclusions

1. A brief survey of the most important phenomena occurring at the solid-liquid interfaces in metal-ceramic systems at high temperatures has been presented, with a special attention to the most recent developments concerning wetting and joining transition metals diborides.
2. The particular case of interactions between liquid metals with early-transition-metal diborides (TiB_2, ZrB_2, HfB_2) has been addressed from both the experimental and theoretical points of view.
3. It has been shown that, at high temperature, the contact angle values and the formation of interfacial dissolution regions are the results of the competition between different phenomena: dissolution of the ceramic in the liquid phase, reaction, formation of new phases at the solid-

liquid interface as well as fast drop spreading along the substrate surface.
4. The presence of surface layers (e.g., oxides) on the UHTC substrates is the main cause of their bad wetting by liquid alloys: oxide elimination can be achieved by imposing proper low oxygen partial pressures and by using active-metals additions.
5. Phase diagrams are essential to show how to suppress the substrate dissolution and how to interpret the evolution of the system as $f(T, Xn_i)$.
6. Sessile-drop experiments can be successfully used to assess critical points of newly calculated phase diagrams: e.g., the formation of compounds, isothermal transitions, and so on.
7. The interaction phenomena have been put in relation with the joining of ceramic and metal-ceramic systems by means of processes in the presence of a liquid phase (brazing, TLPB etc.).
8. These studies are essential for designing joining processes, for creating composite materials, etc., and are of particular relevance when applied to UHTC materials.

Acknowledgments

The authors would like to thank all the colleagues who contributed to this work in recent years, and, in particular, Prof. G. Cacciamani, Dr. C. Artini (DCCI, Unige), and Dr. D. Passerone (Empa, Zurich) as well as their colleagues at IENI Dr. G. Battilana for SEM-EDS analyses and Mr. F. Mocellin for technical support. Figure 8, 9, 11, and 13 are reprinted from Ref 103 and Fig. 20 from Ref 141, with permission from ELSEVIER.

References

1. W.G. Fahrenholtz, E.J. Wuchina, W.E. Lee, and Y. Zhou, Ed., *Ultra-High Temperature Ceramics, Materials for Extreme Environment Applications*, Wiley, Hoboken, 2014
2. E.W. Neuman, G.E. Hilmas, and W.G. Fahrenholtz, Mechanical Behavior of Zirconium Diboride-Silicon Carbide-Boron Carbide Ceramics up to 2200 °C, *J. Eur. Ceram. Soc.*, 2015, **35**, p 463–476
3. J. Zou, G.J. Zhang, C.F. Hu, T. Nishimura, Y. Sakka, J. Vleugels, and O. Biest, Strong ZrB2-SiC-WC Ceramics at 1600 °C, *J. Am. Ceram. Soc.*, 2012, **95**, p 874–878
4. W.G. Fahrenholtz and G.E. Hilmas, Oxidation of Ultra-High Temperature Transition Metal Diboride Ceramics, *Int. Mater. Rev.*, 2012, **57**, p 61–72
5. C.M. Carney, T.A. Parthasarathy, and M.K. Cinibulk, Separating Test Artifacts from Material Behavior in the Oxidation Studies of HfB2-SiC at 2000 °C and Above, *Int. J. Appl. Ceram. Tech.*, 2013, **10**(Ref 2), p 293–300
6. L. Silvestroni, G. Meriggi, and D. Sciti, Oxidation Behavior of ZrB_2 Composites Doped with Various Transition Metal Silicides, *Corros. Sci.*, 2014, **83**, p 281–291
7. M.M. Opeka, I.G. Talmy, and J.A. Zaykoski, Oxidation-Based Materials Selection for 2000 °C + Hypersonic Aerosurfaces: Theoretical Considerations and Historical Experience, *J. Mater. Sci.*, 2004, **39**, p 5887–5904
8. D.M. Wie, D.G. Drewry, Jr., D.E. King, and C.M. Hudson, The Hypersonic Environment: Required Operating Conditions and Design Challenges, *J. Mater. Sci.*, 2004, **39**, p 5915–5924
9. M.F. Morks, I. Cole, and A. Kobayashi, Plasma Forming Multilayer Ceramics for Ultra-High Temperature Application, *Vacuum*, 2013, **88**, p 134–138
10. R.G. Munro, Material Properties of Titanium Diboride, *J. Res. NIST*, 2000, **105**, p 709–720
11. W.G. Fahrenholtz, G.E. Hilmas, I.G. Talmy, and J.A. Zaykoski, Refractory Diborides of Zirconium and Hafnium, *J. Am. Ceram. Soc.*, 2007, **90**, p 1347–1364
12. E. Wuchina, E. Opila, M. Opeka, W.G. Fahrenholtz, and I.G. Talmy, UHTCs: Ultra-High Temperature Ceramic Materials for Extreme Environment Applications, *Interface*, 2007, **16**, p 30–36
13. A. Paul, D.D. Jayaseelan, S. Venugopal, E. Zapata-Solvas, J. Binner, B. Vaid-hyanathan, A. Heaton, P. Brown, and W.E. Lee, UHTC Composites for Hypersonic Applications, *Bull. Am. Ceram. Soc.*, 2011, **91**, p 22–29
14. J.P. Bonal, A. Kohyama, J. Van der Laan, and L.L. Snead, Graphite, Ceramics, and Ceramic Composites for High-Temperature Nuclear Power Systems, *MRS Bull.*, 2009, **34**, p 28–34
15. L. Giancarli, J.P. Bonal, A. Caso, G. Le Marois, N.B. Morly, and J.F. Salavy, Design Requirements for SiC Composites Structural Material in Fusion Power-Reactor Blankets, *Fusion Eng. Design.*, 1998, **41**, p 165–171
16. L. Mercatelli, E. Sani, D. Jafrancesco, J.L. Sans, and E. Sani, Ultra-Refractory Diboride Ceramics for Solar Plant Receivers, *Energy Procedia*, 2014, **49**, p 468–477
17. K. Kuwabara, S. Sakamoto, O. Kida, T. Ishino, T. Kodama, H. Nakajima, T. Ito, and Y. Hirakawa, Corrosion Resistance and Electrical Resistivity of ZrB_2 Monolithic Refractories, in *the Proceedings of UNITECR 2003. The 8th Biennial Worldwide Conference on Refractories, Osaka, Japan*, K. Asano, Ed., (Japan), Technical Association of Refractories, 2003, p 302–305
18. A.M. Weimer, *Carbide, Nitride and Boride Materials, Synthesis and Processing*, Chapman & Hall, London, 1997
19. Z.J. Jin, M. Zhang, D.M. Guo, and R.K. Kang, Electroforming of Copper/ZrB_2 Composites Coatings and Its Performance as Electro-Discharge Machining Electrodes, *Key Eng. Mater.*, 2005, **291–292**, p 537–542
20. P. Luo, S. Dong, Z. Xie, Y. Anzhuo, and Y. Wei, The Effects of Coating Parameters on the Quality of TiB_2-TiC Composite Phase Coating on the Surface of Cu-Cr-Zr Alloy Electrode, *Surf. Coat. Technol.*, 2014, **253**, p 132–138
21. J. Sung, D.M. Goedde, G.S. Girolami, and J.R. Abelson, Remote-Plasma Chemical Vapour Deposition of Conformal ZrB_2 Films at Low Temperature: A Promising Diffusion Barrier for Ultralarge Scale Integrated Electronics, *J. Appl. Phys.*, 2002, **91**, p 3904
22. X. Liang, H. Chuanzhen, L. Hanlian, Z. Bin, Z. Hongtao, Z. Guolong, and W. Jun, In Situ Synthesis of ZrB_2-ZrC_x Ceramic Tool Materials Toughened by Elongated ZrB_2 Grains, *Mater. Design*, 2013, **49**, p 226–233
23. R. Asthana and M. Singh, Active metal Brazing of Advanced Ceramic Composites to Metallic Systems, *Advances in Brazing, Science, technology and applications*, Cambridge, Woodhead Publishing, 2013, p 323-360
24. H.P. Xiong, W. Mao, Y.H. Xie, B. Chen, W.L. Guo, X.H. Li, and Y.Y. Cheng, Control of Interfacial Reactions and Strength of the SiC/SiC Joints Brazed with Newly-Developed Co-Based Brazing Alloy, *J. Mater. Res.*, 2011, **22**, p 2727–2736
25. H.P. Xiong, W. Mao, Y.H. Xie, B. Chen, W.L. Guo, X.H. Li, and Y.Y. Cheng, Brazing of SiC to a Wrought Nickel-Based Superalloy Using CoFeNi(Si, B)CrTi Filler Metal, *Mater. Lett.*, 2007, **61**, p 4662–4665
26. G.O. Cook, III, and C.D. Sorensen, Overview of Transient Liquid Phase and Partial Transient Liquid Phase Bonding, *J. Mater. Sci.*, 2011, **46**, p 5305–5323
27. W.D. MacDonald and T.W. Eagar, Transient Liquid Phase Bonding, *Ann. Rev. Mater. Sci.*, 1992, **22**, p 23–46
28. S.M. Hong, C. Bartlow, T.B. Reynolds, J.T. McKeown, and A.M. Glaeser, Ultrarapid Transient-Liquid-Phase Bonding of Al_2O_3 Ceramics, *Adv. Mater.*, 2008, **20**, p 4799–4803
29. M.L. Shalz, B.J. Dalgleish, and A.P. Tomsia, Ceramic joining, *J. Mater. Sci.*, 1993, **28**, p 1673–1684
30. S.M. Hong, T.B. Reynolds, C.C. Bartlow, and A.M. Glaeser, Rapid Transient-Liquid-Phase Bonding of Al_2O_3 with Microdesigned Ni/Nb/Ni Interlayers, *Int. J. Mater. Res.*, 2010, **101**, p 133–142
31. M.A. Arafin, M. Medraj, D.P. Turner, and P. Bocher, Transient Liquid Phase Bonding of Inconel 718 and Inconel 625 with BNi-2: Modeling and Experimental Investigations, *Mater. Sci. Eng.*, 2007, **A447**, p 125–133
32. M. Pouranvari, A. Ekrami, and A.H. Kokabi, Effect of Bonding Temperature on Microstructure Development During TLP Bonding of a Nickel Base Superalloy, *J. Alloys Compd.*, 2009, **469**, p 270–275

33. G.W. Liu, F. Valenza, M.L. Muolo, and A. Passerone, SiC/SiC and SiC/Kovar Joining by Ni-Si and Mo Interlayers, *J. Mater. Sci.*, 2010, **45**, p 4299–4307
34. L. Esposito, D. Sciti, L. Silvestroni, C. Melandri, S. Guicciardi, N. Saito, K. Nakashima, and A.M. Glaeser, Transient Liquid Phase Bonding of HfC-Based Ceramics, *J. Mater. Sci.*, 2014, **49**, p 654–664
35. I.W. Donald, P.M. Mallinson, B.L. Metcalfe, L.A. Gerrard, and J.A. Fernie, Recent Developments in the Preparation, Characterization and Applications of Glass- and Glass-Ceramic-to-Metal Seals and Coatings, *J. Mater. Sci.*, 2011, **46**, p 1975–2000
36. F. Smeacetto, M. Salvo, F.D. D'Herin Bytner, P. Leone, and M. Ferraris, New Glass and Glass-Ceramic Sealants for Planar Solid Oxide Fuel Cells, *J. Eur. Ceram. Soc.*, 2010, **30**, p 933–940
37. M. Salvo, V. Casalegno, S. Rizzo, F. Smeacetto, A. Ventrella, and M. Ferraris, Glasses and Glass-Ceramics as Brazing Materials for High-Temperature Applications, *Advances in Brazing: Science, Technology and Applications*, D.P. Sekulic, Ed., Book Series: Woodhead Publishing Series in Welding and Other Joining Technologies Issue: 80, 2013, p 525-544
38. Q.G. Fu, H.J. Li, P.H. Feng, and X.Y. Nan, A Gradient LMAS Interlayer Joint of SiC Coated C/C Composites to LAS Glass Ceramics, *Ceram. Int.*, 2014, **40(B)**, p 2461–2466
39. R. Asthana and N. Sobczak, Wettability in Joining of Advanced Ceramics and Composites: Issues and Challenges, *Ceram. Trans.*, 2014, **248**, p 591–600
40. M. Herrmann, W. Lippmann, and A. Hurtado, Y_2O_3-Al_2O_3-SiO_2-Based Glass-Ceramic Fillers for the Laser-Supported Joining of SiC, *J. Eur. Ceram. Soc.*, 2014, **34**, p 1935–1948
41. N. Sobczak, M. Singh, and R. Asthana, High-Temperature Wettability Measurements in Metal/Ceramic Systems—Some Methodological Issues, *Curr. Opin. Solid State Mater. Sci.*, 2005, **9**, p 241
42. E. Saiz and A.P. Tomsia, Atomic Dynamics and Marangoni Films During Liquid-Metal Spreading, *Nature Mater.*, 2004, **3**, p 903–909
43. A. Passerone, M.L. Muolo, F. Valenza, F. Monteverde, and N. Sobczak, Wetting and Interfacial Phenomena in Ni-HfB_2 Systems, *Acta Mater.*, 2009, **75**, p 356–364
44. M.L. Muolo, E. Ferrera, R. Novakovic, and A. Passerone, Wettability of Zirconium Diboride Ceramics by Ag, *Scr. Mater.*, 2003, **48**, p 191–196
45. N.Y. Naidich, V.S. Zhuravlev, I.I. Gab, B.D. Kostyuk, V.P. Krasovskyy, A.A. Adamovskyy, and N.Y. Taranets, Liquid Metal Wettability and Advanced Ceramic Brazing, *J. Eur. Ceram. Soc.*, 2008, **28**, p 717–728
46. V. Bougiouri, R. Voytovych, O. Dezellus, and N. Eustathopoulos, Wetting and Reactivity in Ni-Si/C System: Experiments Versus Model Predictions, *J. Mater. Sci.*, 2007, **42**, p 2016–2023
47. P. Prakash, T. Mohandas, and P.D. Raju, Microstructural Characterization of SiC Ceramic and SiC-Metal Active Metal Brazed Joints, *Scr. Mater.*, 2005, **52**, p 1169–1173
48. B. Chen, H.P. Xiong, W. Mao, W.L. Guo, Y.Y. Cheng, and X.X. Li, Microstructure and Property of SiC-SiC Joints Brazed with PdNi-Cr-V Brazing Filler, *Acta Metall. Sin.*, 2007, **43**, p 1181–1185
49. G.W. Liu, G.J. Qiao, H.J. Wang, J.F. Yang, and T.J. Lu, Pressureless Brazing of Zirconia to Stainless Steel with Ag-Cu Filler Metal and TiH_2 Powder, *J. Eur. Ceram. Soc.*, 2008, **28**, p 2701–2708
50. G.W. Liu, W. Li, G.J. Qiao, H.J. Wang, J.F. Yang, and T.J. Lu, Microstructures and Interfacial Behavior of Zirconia/Stainless Steel Joint Prepared by Pressureless Active Brazing, *J. Alloys Compd.*, 2009, **470**, p 163
51. M.L. Hattali, S. Valette, F. Ropital, N. Mesrati, and D. Treheux, Effect of Thermal Residual Stresses on the Strength for Both Alumina/Ni/Alumina and Alumina/Ni/Nickel Alloy Bimaterials, *J. Mater. Sci.*, 2009, **44**, p 3198–3220
52. S.J. Li, Y. Zhou, H.P. Duan, J.H. Qiu, and Y. Zhang, Joining of SiC Ceramic to Ni-Based Superalloy with Functionally Gradient Material Fillers and a Tungsten Intermediate Layer, *J. Mater. Sci.*, 2003, **38**, p 4065–4070
53. S. Buhl, C. Leinenbach, R. Spolenak, and K. Wegener, Microstructure, Residual Stresses and Shear Strength of Diamond-Steel-Joints Brazed with a Cu-Sn-Based Active Filler Alloy, *Int. J. Refract. Met. Hard Mater.*, 2012, **30**, p 16–24
54. H.J. Schindler and C. Leinenback, Mechanics of fatigue crack growth in a bonding interface, *Eng. Fract. Mech.*, 2012, **89**, p 52–64
55. M. Benhassine, E. Saiz, A.P. Tomsia, and J. De Coninck, Nonreactive Wetting Kinetics of Binary Alloys: A Molecular Dynamics Study, *Acta Mater.*, 2011, **59**, p 1087–1094
56. E.B. Webb, III, G.S. Grest, D.R. Heine, and J.J. Hoyt, Dissolutive Wetting of Ag on Cu: a Molecular Dynamics Simulation Study, *Acta Mater.*, 2005, **53**, p 3163–3177
57. E. Bertrand, T.D. Blake, and J. De Coninck, Influence of Solid-Liquid Interactions on Dynamic Wetting: A Molecular Dynamics Study, *J. Phys. Condens. Matter*, 2009, **21**, p 464124
58. M.W. Finnis, The Theory of Metal-Ceramic Interfaces, *J. Phys. Condens. Matter*, 1996, **8**, p 811–5836
59. A.E. Mattsson, P.A. Schultz, M.P. Desjarlais, T.R. Mattsson, and K. Leung, Designing Meaningful Density Functional Theory Calculations in Materials Science—A Primer, *Modell. Simul. Mater. Sci. Eng.*, 2005, **13**, p R1–R31
60. R. Goswami, C.S. Pande, N. Bernstein, M.D. Johannes, C. Baker, and G. Villalobos, A High Degree of Enhancement of Strength of Sputter Deposited Al/Al_2O_3 Multilayers Upon Post Annealing, *Acta Mater.*, 2015, **95**, p 378–385
61. E. Glickman, D. Fuks, N. Frage, S. Barzilai, and N. Froumin, Adsorption Effect in Non-reaction Wetting: In-Ti on CaF_2, *Appl. Phys. A Mater. Sci. Proc.*, 2012, **106**, p 181–189
62. M.L. Muolo, F. Valenza, A. Passerone, and D. Passerone, Oxygen Influence on Ceramics Wettability by Liquid Metals: Ag/α-Al_2O_3-Experiments and Modelling, *J. Mater. Sci. Eng. A*, 2008, **495**, p 153–158
63. A. Hashibon and C. Elsässer, Approaches to Atomistic Triple-Line Properties from First-Principles, *Scr. Mater.*, 2010, **62**, p 939–944
64. D. Passerone, C.A. Pignedoli, F. Valenza, M.L. Muolo, and A. Passerone, Ab initio Simulations of the Ag(111)/Al_2O_3 Interface at Intermediate Oxygen Partial Pressures, *J. Mater. Sci.*, 2010, **45**, p 4265–4270
65. S.E. Kulkova, A.V. Bakulin, S. Hocker, and S. Schmauder, Theoretical Study of Adhesion at the Metal-Zirconium Dioxide Interfaces, *Technol. Phys.*, 2013, **58**, p 325–334
66. S.V. Dudiy and B.I. Lundqvist, Wetting of TiC and TiN by Metals, *Phys. Rev. B*, 2004, **69**, p 125421
67. A.V. Bakulin and S.E. Kulkova, Theoretical Study of the Adsorption of 3d- and 4d-Metals on a WC(0001) Surface, *J. Exp. Theor. Phys.*, 2013, **117**, p 309–319
68. G. Feldbauer, M. Wolloch, P.O. Bedolla, P. Mohn, J. Redinger, and A. Vernes, Adhesion and Material Transfer Between Contacting Al and TiN Surfaces from First Principles, *Phys. Rev. B*, 2015, **91**, p 165413
69. M.L. Liu, S.Q. Wang, and H.Q. Ye, First-Principles Study of Metal/Nitride Polar Interfaces: Ti/TiN, *Surf. Interface Anal.*, 2003, **35**, p 835–841
70. S.K. Yadav, R. Ramprasad, J. Wang, A. Misra, and X.Y. Liu, First-Principles Study of Cu/TiN and Al/TiN Interfaces: Weak Versus Strong Interfaces, *Modell. Sim. Mater. Sci. Eng.*, 2014, **22**, p 035020
71. A. Passerone, M.L. Muolo, and D. Passerone, Wetting of Group IV Diborides by Liquid Metals, *J. Mater. Sci.*, 2006, **41**, p 5088–5098
72. H.Y. Wang, S. Zhang, D.J. Li, and S.Y. Liu, The Simulation of Adhesion, Stability, Electronic Structure of W/ZrB2 Interface Using First-Principles, *Surf. Coat. Technol.*, 2013, **228**, p S583–S587
73. A. Passerone, M.L. Muolo, R. Novakovic, and D. Passerone, Liquid Metal/Ceramic Interactions in the (Cu, Ag, Au)/ZrB_2 Systems, *J. Eur. Ceram. Soc.*, 2007, **27**, p 3277–3285
74. K. Luo, Q. Deng, X. Zha, Q. Huang, J.S. Francisco, X. Yu, Y. Qiao, J. He, and S. Du, Electronic Structures and Mechanical Properties of Al(111)/ZrB_2 (0001) Heterojunctions from First-Principles Calculation, *Mol. Phys.*, 2015, **113**, p 1794–1801
75. N. Eustathopoulos, M.G. Nicholas, and B. Drevet, *Wettability at High Temperature, Pergamon Materials Series*, Elsevier, Oxford, 1999
76. N. Eustathopoulos, N. Sobczak, A. Passerone, and K. Nogi, Measurement of Contact Angle and Work of Adhesion at High Temperature, *J. Mater. Sci.*, 2005, **40**, p 2271–2280
77. E. Saiz, M. Benhassine, J. De Coninck, and A.P. Tomsia, Early Stages of Dissolutive Spreading, *Scr. Mater.*, 2010, **62**, p 934–938
78. E. Saiz, R.M. Cannon, and A.P. Tomsia, Reactive Spreading: Adsorption, Ridging and Compound Formation, *Acta Mater.*, 2000, **48**, p 4449–4462
79. V. Voué and J. De Coninck, Spreading and Wetting at the Microscopic Scale: Recent Developments and Perspectives, *Acta Mater.*, 2000, **48**, p 4405–4417

80. O. Dezellus, F. Hodaj, and N. Eustathopoulos, Chemical Reaction-Limited Spreading: The Triple Line Velocity Versus Contact Angle Relation, *Acta Mater.*, 2002, **50**, p 4741–4753
81. E.B. Webb, III, J.J. Hoyt, and G.S. Grest, High Temperature Wetting: Insights from Atomistic Simulations, *Curr. Opin. Solid State Mater. Sci.*, 2005, **9**, p 174–180
82. D. Chatain and W.C. Carter, Wetting Dynamics. Spreading of Metallic Drops, *Nature Mater.*, 2004, **3**, p 843–845
83. G. Kumar and K.N. Prabhu, Review of Non-reactive and Reactive Wetting of Liquids on Surfaces, *Adv. Colloid Interface Sci.*, 2007, **133**, p 61–89
84. O. Dezellus and N. Eustathopoulos, Fundamental Issues of Reactive Wetting by Liquid Metals, *J. Mater. Sci.*, 2010, **45**, p 4256–4264
85. E.B. Webb, III, and J.J. Hoyt, Molecular Dynamics Study of Liquid Metal Infiltration During Brazing, *Acta Mater.*, 2008, **56**, p 1802–1812
86. W. Tillmann, J. Pfeiffer, N. Sievers, and K. Boettcher, Analyses of the Spreading Kinetics of AgCuTi Melts on Silicon Carbide Below 900 °C, Using a Large-Chamber SEM, *Colloids Surf. A Physicochem. Eng. Aspects*, 2015, **468**, p 167–173
87. Q. Lin and R. Cao, Characteristics of Spreading Dynamics for Adsorption Wetting at High Temperatures, *Compd. Mater. Sci.*, 2015, **99**, p 29–32
88. T.J. Singler, S. Su, L. Yin, and B.T. Murray, Modeling and Experiments in Dissolutive Wetting: A Review, *J. Mater. Sci.*, 2012, **47**, p 8261–8274
89. L. Yin, B.T. Murray, S. Su, Y. Sun, Y. Efraim, H. Taitelbaum, and T.J. Singler, Reactive Wetting in Metal-Metal Systems, *J. Phys. Condens. Matter*, 2009, **21**, p 464130
90. P. Protsenko, J.P. Garandet, R. Voytovych, and N. Eustathopoulos, Thermodynamics and Kinetics of Dissolutive Wetting of Si by Liquid Cu, *Acta Mater.*, 2010, **58**, p 6565–6574
91. O. Kozlova, R. Voytovych, P. Protsenko, and N. Eustathopoulos, Non-reactive Versus Dissolutive Wetting of Ag-Cu Alloys on Cu Substrates, *J. Mater. Sci.*, 2010, **45**, p 2099–2105
92. W. Villanueva, W.J. Boettinger, G. McFadden, and J.A. Warren, A Diffuse-Interface Model of Reactive Wetting with Intermetallic Formation, *Acta Mater.*, 2012, **60**, p 3799–3814
93. S. Su, L. Yin, Y. Sun, B.T. Murray, and T.J. Singler, Modeling Dissolution and Spreading of Bi-Sn Alloy Drops on a Bi Substrate, *Acta Mater.*, 2009, **57**, p 3110–3122
94. L. Yin, A. Chauhan, and T.J. Singler, Reactive Wetting in Metal/Metal Systems: Dissolutive Versus Compound-Forming Systems, *Mater. Sci. Eng. A*, 2008, **495**, p 80–89
95. P. Protsenko, O. Kozlova, R. Voytovych, and N. Eustathopoulos, Dissolutive Wetting of Si by Molten Cu, *J. Mater. Sci.*, 2008, **43**, p 5669–5671
96. L. Yin, B.T. Murray, and T.J. Singler, Dissolutive Wetting in the Bi-Sn System, *Acta Mater.*, 2006, **4**, p 3561–3574
97. E. Saiz, A.P. Tomsia, and R.M. Cannon, Ridging Effects on Wetting and Spreading of Liquids on Solids, *Acta Mater.*, 1998, **46**, p 2349–2361
98. E. Saiz, R.M. Cannon, and A.P. Tomsia, Energetics and Atomic Transport at Liquid Metal/Al_2O_3 Interfaces, *Acta Mater.*, 1999, **47**, p 4209–4220
99. G. Levi and W.G. Kaplan, Aluminium-Alumina Interface Morphology and Thermodynamics from Dewetting Experiments, *Acta Mater.*, 2003, **51**, p 2793–2802
100. E. Saiz, A.P. Tomsia, and R.M. Cannon, Triple Line Ridging and Attachment in High Temperature Wetting, *Scr. Mater.*, 2001, **44**, p 159–164
101. G. Levi, C. Scheu, and W.D. Kaplan, Segregation of Aluminium at Nickel-Sapphire Interfaces, *Interface Sci.*, 2001, **9**, p 213–220
102. C.X. Zheng, W.X. Tang, and D.E. Jesso, Asymmetric Coalescence of Reactively Wetting Droplets, *Appl. Phys. Lett.*, 2012, **100**, p 071903
103. A. Passerone, M.L. Muolo, F. Valenza, and L. Kaufman, Wettability of HfB_2 by Molten Ni(B) Alloys Interpreted by CALPHAD Methods. Part 2, Wetting and Interfacial Reactivity, *CALPHAD*, 2010, **34**, p 6–14
104. P. Erhardt and S.H. Davis, Non-isothermal Spreading of Liquid Drops on Horizontal Plates, *J. Fluid Mech.*, 1991, **229**, p 229–365
105. B. Komolafe and M. Medraj, Progress in Wettability Study of Reactive Systems, *J. Metall.*, 2014, **2014**(387046), p 14
106. N. Eustathopoulos and R. Voytovych, The Role of Reactivity in Wetting by Liquid Metals: A Review, *J. Mater. Sci.*, 2016, **51**, p 425–437
107. C. Iwamoto and S. Tanaka, Atomic Morphology and Chemical Reactions of the Reactive Wetting Front, *Acta Mater.*, 2002, **50**, p 749–755
108. A.H. Carim, Convergent-Beam Electron Diffraction "Fingerprinting" of M_6X Phases at Brazed Ceramic Joints, *Scr. Metall. Mater.*, 1991, **25**, p 51–54
109. A.H. Carim and C.H. Mohr, Brazing of Alumina with Ti_4Cu_2O and Ti_3Cu_3O Interlayers, *Mater. Lett.*, 1997, **33**, p 195–199
110. M. Aizenshtein, N. Froumin, and N. Frage, Experimental Study and Thermodynamic Analysis of High Temperature Interactions between Boron Carbide and Liquid Metals, *Engineering*, 2014, **6**, p p849–p868
111. W.J. Boettinger, C.A. Handwerker, and U.R. Kattner, Reactive Wetting and Intermetallic Formation, *The Mechanics of Solder Alloy Wetting and Spreading*, F.G. Yost, F.M. Hosking, and D.R. Frear, Ed., Van Nostrand Reinhold, New York, 1993, p 103–139
112. R.N. Wenzel, Resistance of Solid Surfaces to Wetting by Water, *Ind. Eng. Chem.*, 1936, **28**, p 988–994
113. R. David and A.W. Neumann, Energy Barriers Between the Cassie and Wenzel States on Random, Superhydrophobic Surfaces, *Colloids Surf. A Physicochem. Eng. Aspects*, 2013, **425**, p 51–58
114. A.B.D. Cassie and S. Baxter, Wettability of Porous Surfaces, *Trans. Faraday Soc.*, 1944, **40**, p 546–551
115. A.B.D. Cassie, Contact Angles, *Discuss. Faraday Soc.*, 1948, **3**, p 11
116. G.V. Samsonov and I.M. Vinitskii, *Handbook of Refractory Compounds*, IFI/Plenum, New York, 1980
117. Y.V. Naidich, The Wettability of Solids by Liquid Metals, *Progress in Surface and Membrane Science*, Vol 14, D.A. Cadenhead et al., Eds., Academic Press, New York, 1981, p 353–492
118. P. Xiao and B. Derby, Wetting of TiN and TiC by Liquid Metals, *Acta Mater.*, 1996, **44**, p 307–314
119. S. Lequeux, F. Le Guyadec, M. Berardo, L. Coudurier, and N. Eustathopoulos, Wetting and Interfacial Reactions of Cu and Cu Alloys on TiN, *Proc. 2nd Int. Conf. High Temp. Capillarity*, N. Eustathopoulos, and N. Sobczak, Eds., FRI Cracow, Poland, 1997, p 112-117
120. M.L. Muolo, M. Bassoli, B. Wollein, W. Lengauer, and A. Passerone, Wetting of TiN by Liquid Copper, *Trans. JWRI*, 2001, **30**, p 49–54
121. S. Kalogeropoulos, J. Van Deelen, N. Eustathopoulos, F. Le Guyadec, and M. Berardo, Study of Cu/TiN System, Wetting or Non-wetting, *Trans. JWRI*, 2001, **30**, p 107–112
122. N. Frage, N. Froumin, and M.P. Dariel, Wetting of TiC by Non-reactive Liquid Metals, *Acta Mater.*, 2002, **50**, p 237–245
123. S.M. McDeavitt, G.W. Billings, and J.E. Indacochea, High Temperature Interaction Behavior at Liquid Metal-Ceramic Interfaces, *J. Mater. Eng. Perform.*, 2002, **11**, p 392–401
124. N. Frage, N. Froumin, M. Alzenshtein, L. Kutsenko, D. Fucks, and M.P. Dariel, Reactive Wetting in Titanium Carbide/Non-reactive Metal Systems, *Curr. Opin. Solid State Mater. Sci.*, 2005, **9**, p 189–195
125. M. Aizenshtein, N. Froumin, P. Barth, E. Shapiro-Tsoref, M.P. Dariel, and N. Frage, How Does the Composition of Quasi-Stoichiometric Titanium Diboride Affect Its Wetting by Molten Cu and Au?, *J. Alloys Compd.*, 2007, **442**, p 375–378
126. A.V. Durov, Y.V. Naidich, and B.D. Kostyuk, Investigation of Interaction of Metal Melts and Zirconia, *J. Mater. Sci.*, 2005, **40**, p 2173–2178
127. T.P. Swiler and R.E. Loehman, Molecular Dynamics Simulations of Reactive Wetting in Metal-Ceramic Systems, *Acta Mater.*, 2000, **48**, p 4419–4424
128. S. Khan, G. Azimi, B. Yildiz, and K.K. Varanasi, Role of Surface Oxygen-to-Metal Ratio on the Wettability of Rare-Earth Oxides, *Appl. Phys. Lett.*, 2015, **106**, p 061601
129. G.J. Zhang, H.T. Liu, W.W. Wu, J. Zou, D.W. Ni, W.M. Guo, J.X. Liu, and X.G. Wang, Reactive Processes for Diboride Based UHTC, in Ref 1, Ch. 3, p 33
130. M. Scheer, The Molecular Weight and Vapour Pressure of Gaseous Boron Suboxide, *J. Phys. Chem.*, 1958, **62**, p 490–493
131. L. Kaufman, G. Cacciamani, M.L. Muolo, F. Valenza, and A. Passerone, Wettability of HfB_2 by Molten Ni(B) Alloys Interpreted by

CALPHAD Methods. Part 1, Definition of the B-Hf-Ni System, *CALPHAD*, 2010, **34**, p 2–5
132. M. Aizenshtein, N. Froumin, and N. Frage, The Nature of TiB_2 Wetting by Cu and Au, *J. Mater. Eng. Perform.*, 2012, **21**, p 655–659
133. A. Passerone, F. Valenza, and M.L. Muolo, A Review of Transition Metals Diborides: From Wettability Studies to Joining, *J. Mater. Sci.*, 2012, **47**, p 8275–8289
134. L. Xi, I. Kaban, R. Novak, B. Korpala, G. Brudzda, N. Sobczak, N. Mattern, and J. Eckert, High-Temperature Wetting and Interfacial Interaction Between Liquid Al and TiB_2 Ceramic, *J. Mater. Sci.*, 2015, **50**, p 2682–2690
135. N. Sobczak, R. Nowak, W. Radziwill, J. Budziok, and A. Glenz, Experimental Complex for Investigations on High Temperature Capillarity Phenomena, *Mater. Sci. Eng. A*, 2008, **495**, p 43–49
136. O. Umanskyi, O. Poliarus, M. Ukrainets, and M. Antonov, Physical-Chemical Interaction in NiAl-MeB_2 Systems Intended for Tribological Applications, *Weld. J.*, 2015, **94**, p 225–230
137. V.P. Konoval, Zh Shemet, B. Grushko, A.D. Panasyuk, T.V. Mosina, and V.I. Subbotin, Refractory and Ceramic Materials Structure and Properties of Ti-Cr Diboride Composites, *Powder Metall. Metal Ceram.*, 2012, **51**, p 429–436
138. G.L. Zhunkovkii, T.M. Evtushok, O.N. Grigor'ev, and P.V. Mazur, Activated Sintering of Refractory Borides, *Powder Metall. Metal Ceram.*, 2011, **50**, p 212–216
139. F. Valenza, M.L. Muolo, A. Passerone, G. Cacciamani, and C. Artini, Control of Interfacial Reactivity Between ZrB_2 and Ni-Based Brazing Alloys, *J. Mater. Eng. Perform.*, 2012, **21**, p 660–666
140. G. Cacciamani, P. Riani, and F. Valenza, Equilibrium Between MB_2 (M = Ti, Zr, Hf) UHTC and Ni: A Thermodynamic Database for the B-Hf-Ni-Ti-Zr System, *CALPHAD*, 2011, **35**, p 601–619
141. C. Artini, M.L. Muolo, A. Passerone, G. Cacciamani, and F. Valenza, Isothermal Solid-Liquid Transitions in the (Ni, B)/ZrB_2 System as Revealed by Sessile Drop Experiments, *J. Mater. Sci.*, 2013, **48**, p 5029–5035
142. C. Artini, M.L. Muolo, A. Passerone, F. Valenza, P. Manfrinetti, and G. Cacciamani, Experimental Investigations and Thermodynamic Modeling in the ZrB_2-Ni Section of the BNiZr System, *J Alloys Compd.*, 2014, **592**, p 115–120
143. R. Asthana and M. Singh, Evaluation of Amorphous Ti Brazes to Join Zirconium Diboride-Based Ultra-High-Temperature Ceramics to Metallic Systems, *Int. J. Appl. Ceram. Technol.*, 2014, **11**, p 502–512
144. R. Asthana and M. Singh, Joining of ZrB_2-Based Ultra-High-Temperature Ceramic Composites Using Pd-Based Braze Alloys, *Scr. Mater.*, 2009, **61**, p 257–260
145. M. Singh and R. Asthana, Joining and Integration of ZrB_2-Based Ultra-High Temperature Ceramic Composites Using Advanced Brazing Technology, *J. Mater. Sci.*, 2010, **45**, p 4308–4320
146. N. Saito, H. Ikeda, Y. Yamaoka, A.M. Glaeser, and K. Nakashima, Wettability and Transient Liquid Phase Bonding of Hafnium Diboride Composite with Ni-Nb Alloys, *J. Mater. Sci.*, 2012, **47**, p 8454–8463
147. W. Yang, P. He, L. Xing, and T. Lin, Microstructural Evolution and Mechanical Properties of ZrB_2-SiC/Cu/Ti/Ti6Al4V Brazing Joints, *Adv. Eng. Mater.*, 2015, **17**, p 1556–1561
148. W. Yang, T. Lin, P. He, M. Zhu, C. Song, D. Jia, and J. Feng, Microstructural Evolution and Growth Behavior of *In Situ* TiB Whisker Array inZrB_2-SiC/Ti6Al4V Brazing Joints, *J. Am. Ceram. Soc.*, 2013, **96**, p 3712–3719
149. W.R. Pinc, M. Di Prima, L.S. Walker, Z.N. Wing, and E.L. Corral, Spark Plasma Joining of ZrB_2-SiC Composites Using Zirconium-Boron Reactive Filler Layers, *J. Am. Ceram. Soc.*, 2011, **94**, p 3825–3832
150. W. Yang, P. He, T. Lin, C. Song, R. Li, and D. Jia, Diffusion Bonding of ZrB_2-SiC and Nb Using Dynamic Compressed Ni Foam Interlayer, *Mater. Sci. Eng. A*, 2013, **573**, p 1–6
151. F. Valenza, C. Artini, A. Passerone, and M.L. Muolo, ZrB_2-SiC/Ti6Al4V Joints: Wettability Studies Using Ag- and Cu-Based Braze Alloys, *J. Mater. Sci.*, 2012, **47**, p 8439–8449
152. F. Valenza, C. Artini, A. Passerone, P. Cirillo, and M.L. Muolo, Joining of ZrB_2 Ceramics to Ti6Al4V by Ni-Based Interlayers, *J. Mater. Eng. Perform.*, 2014, **23**, p 555–1560